Quaternary Science Reviews 291 (2022) 107662

Contents lists available at ScienceDirect

Quaternary Science Reviews

journal homepage: www.elsevier.com/locate/quascirev

Lessons from a lakebed: unpicking hydrological change and early human landscape use in the Makgadikgadi basin, Botswana

Sallie L. Burrough [a, *], David S.G. Thomas [b, c], Joshua R. Allin [b], Sheila D. Coulson [d], Sarah M. Mothulatshipi [e], David J. Nash [c, f], Sigrid Staurset [b]

[a] Environmental Change Institute, University of Oxford, South Parks Road, Oxford, OX1 3QY, United Kingdom
[b] School of Geography and Environment, University of Oxford, South Parks Road, Oxford, OX1 3QY, United Kingdom
[c] School of Geography, Archaeology and Environmental Studies, University of the Witwatersrand, South Africa
[d] Institute of Archaeology, Conservation and History, University of Oslo, Blindernveien 11, 0315, Oslo, Norway
[e] Department of History, University of Botswana, Private Bag UB, 0022, Gaborone, Botswana
[f] School of Applied Sciences, University of Brighton, Lewes Road, Brighton, BN2 4GJ, United Kingdom

ARTICLE INFO

Article history:
Received 21 December 2021
Received in revised form
8 June 2022
Accepted 23 June 2022
Available online 8 August 2022

Handling Editor: David S G Thomas

Keywords:
Kalahari
Archaeology
Stone age
Palaeolake
Salt pan
MSA

ABSTRACT

The intersection of archaeological material with the landscape is investigated using OSL dating of landforms associated with Middle Stone Age (MSA) archaeology in the Makgadikgadi basin, Botswana. In this study, MSA archaeological sites on the Makgadikgadi pan floor date to two dry periods in the basin during the late Quaternary. Site formation at one site occurred during dry, or seasonally dry conditions that followed a period of high lake levels between 128 ± 18 ka and 81 ± 6 ka. The site was buried by sediments from a subsequent period of high lake levels dating to between 72 ± 5 ka and 57 ± 8 ka. At other investigated sites, the archaeological material was most likely deposited during a second dry period sometime after this. Overlying dunes are much younger (late Holocene) than the late Pleistocene lakebed sediments associated with the archaeological sites. Rapid burial of the archaeological sites by clayey sands has resulted in limited disturbance and weathering of archaeological material which appears to have only been exposed very recently, perhaps in the last 350 years when conditions have been particularly dry and susceptible to deflation. The spatial patterning of both sediment accumulation and deflation strongly influences archaeological visibility both within and around the Makgadikgadi basin.

1. Introduction

Over the last few decades, there has been strong interest in examining the link between long term trends and events in African palaeoenvironments and observations in the African Stone Age archaeological record (e.g., Scholz et al., 2007; Jacobs and Roberts, 2009; Stager et al., 2011). Archaeological observations relate to both landscape and resource use and have focused particularly on the geographical distribution of early modern humans and their dispersal both within and out of Africa (e.g. (Roberts et al., 2020; Scerri and Spinapolice, 2019; Viehberg et al., 2018). The influence of aridity on human resource use and mobility is often emphasized (e.g. Chase et al., 2018), though the spatial complexities of both landscape and climate dynamics are frequently neglected (Burrough, 2016; Thomas et al., 2012). In southern Africa, the historic focus of research has been on coastal cave sites, not least because these settings offer a repeated or continuous occupation record, capturing millennia of human dynamics. More recently however, there has been a recognition that, despite the extraordinary value of these records, the heavy weighting of archaeological evidence derived from them may skew our window into the human past and bias interpretations of landscape, environment, and resource use by ancestral humans. Humans may not have undertaken similar activities in caves compared to the open landscape of the interior. The availability and predictability of resources was also likely controlled by very different factors away from the coast. At coastal cave sites, sea-level rises and falls (as defined by Marine Oxygen Isotope Stages) would have caused changes to the distribution of marine and terrestrial resources (Marean et al., 2020). In contrast, in the interior, glacial/interglacial phases may have acted only to modulate aridity/humidity variables through the impact directly on temperature and indirectly on precession control of the

* Corresponding author.
E-mail address: sallie.burrough@ouce.ox.ac.uk (S.L. Burrough).

https://doi.org/10.1016/j.quascirev.2022.107662

tropical rainbelt (Singarayer and Burrough, 2015). The deficit of research into open air sites in the southern African interior is largely a corollary of the nature of the environment. Its geological history and relative aridity have generated little opportunity for the preservation of organic material and, within the Kalahari basin, very few archaeological sites are visible at the surface of the deep sand environment. Nevertheless, where open air sites are being systematically investigated on the margins of the Kalahari basin (e.g. Chazan et al., 2012; Ecker et al., 2021; Helgren and Brooks, 1983; Lukich et al., 2020; Schoville et al., 2022; Papadimitrios et al., 2019; Walker et al., 2014; Wilkins, 2017, 2021) they are beginning to provide glimpses into Stone Age life in landscapes where environmental trends and resource strategies took a different trajectory to those of the southern Cape coastal region.

In this study, OSL dating of sediments from landforms associated with open-air Stone Age archaeological sites in the Makgadikgadi basin, northern Botswana, are used to determine the timing of both landform development and human occupation of the palaeolake basin. This is critical in light of hypotheses generated by genetic studies that this region constitutes the 'homeland' of Anatomically Modern Humans (AMH) (Chan et al., 2019). Such ideas are highly controversial, but the region lacks systematic archaeological investigations with strong chronological control to refute or support these genetic data. The intersection of landscape archaeology and palaeohydrological research enables us to both shed light on the Kalahari's human prehistory (Staurset et al., 2022a) as well as address how the landscape impacts archaeological visibility, providing greater insight for targeted archaeological studies within this and similar environments in the future. Dating the archaeological sites within the margins of the palaeolake, and associations with surrounding landforms, also provides much needed context on the evolution of the landscape. This allows us to move forward longstanding debates concerning whether the presence of Stone Age archaeology on the Makgadikgadi lake floor can be used as evidence for the absence of lake level fluctuations since site formation (section 2.2).

2. The Makgadikgadi basin

Visible from space, the Makgadikgadi is a salt pan at the heart of the Kalahari basin forming the terminal sump of rivers that seasonally supply water into the continental interior during the dry austral winter months (May–September) from tropical wetlands more than 1000 km to the northwest. Today, it is water from the Okavango that occasionally makes its way into the Makgadikgadi basin via the Boteti River but, in the past, there may have been contributions from a much wider catchment via both the Kwando and Upper Zambezi. The salt pan also receives locally derived flow during the austral summer from ephemeral rivers that drain the area east and northeast of the Makgadikgadi. Many migratory species within the continental interior, particularly ungulates, are highly dependent on the hydrological regime of Okavango/Boteti system (e.g. Bartlam-Brooks et al., 2011). The seasonal climate further drives predictable herbivore and bird migrations into and out of the pans (Bradley, 2012; Mcculloch, 2004; Naidoo et al., 2016), which have long been important to a broad range of predators, not least humans (e.g. Hitchcock et al., 2019). Ethnographic research suggests the predictability of this seasonal resource availability has strongly affected not only human landscape use, in terms of the longevity and repetitive occupation of wetter areas in dry environments but has impacted the archaeological visibility of these locations (Brooks, 1984). Archaeological visibility close to water resources is further amplified within the Middle Kalahari because of the erosive nature of fluvial systems and deflationary dry lakebeds (Vickery et al., 2013). The probability of exposed archaeological sites and stratigraphy associated with these landforms is much higher when compared to the surrounding deep accumulations of vegetated Kalahari sands that might cover or obscure the visibility of archaeological deposits. It is no surprise then, that archaeological material from the Stone Age to the present has been observed extensively within the Makgadikgadi basin and its inflows (see Burrough, 2016; Wilkins, 2021; Coulson et al., 2022). Critical questions however, regarding both *when* and *how* Stone Age humans were using the basin and how their presence in the landscape intersected with Makgadikgadi's hydrological history, have remained unanswered.

2.1. Origin and evolution of the Makgadikgadi basin

The origins of Makgadikgadi are uncertain but it seems likely that the basin formed as a consequence of separation of fluvial systems within the Kalahari basin from the easterly-flowing Limpopo drainage (Du Toit, 1933), due to uplift along the Kalahari-Zimbabwe axis (Moore, 1999) (Fig. 1). This allowed water and sediment that previously discharged into the Indian Ocean to accumulate in the region of the Makgadikgadi basin as rivers flowing from the north (principally the Okavango and Zambezi systems) terminated in the Kalahari interior. The timing of uplift is uncertain but Pliocene-age pollen in fluvio-lacustrine deposits overlying the Makgadikgadi basement provides a maximum age for the initiation of lacustrine sedimentation (Moore et al., 2012). Superimposed on this process, the gradual extension of the east African Rift System (EARS), and the associated downwarping that formed the Okavango depression to its southwest (Vainer et al., 2021) strongly affected the landscape of what is now northern Botswana. Importantly, this included progressively reorganising the northeasterly drainage systems that contributed flow to the interior, with profound hydrological and geomorphological consequences for Makgadikgadi. Uplift along the Chobe Fault across the Upper Zambezi diverted the Palaeo-Chambeshi/Upper Zambezi system into northern Botswana (Moore et al., 2012), creating a drainage configuration associated with Makgadikgadi's largest former lacustrine phase, *Palaeo-Lake Deception* (McFarlane and Eckardt, 2006). Sometime after this, the lake's catchment size shrank as the link between the Chambeshi and Kafue systems was severed by uplift of the Congo-Zambezi watershed (Cotterill and De Wit, 2011). Other major changes initiated by tectonic activity included uplift along the Linyanti fault, diverting the Cuando into the Zambezi via the Chobe (Moore et al., 2012), and the tectonically induced capture of the upper Zambezi by the middle Zambezi. The timing of many of these events is poorly constrained, but the tectonism-driven reorganization of these river systems resulted in a progressively shrinking palaeolake during the Quaternary.

2.2. Models of late quaternary kalahari palaeolake dynamics

It is during the late Quaternary that interpretations of the hydrological history of Makgadikgadi diverge into two different schools of thought, based on apparently opposing evidence. The result, accordingly, is two very different hydroclimate and environmental records for the Kalahari region more widely. These can be broadly summarised as two models:

i) The Quiescent model: Deprived of its major inflows, the basin dried out and remained largely inactive over the late Quaternary, with the exception of neotectonic modifications to its existing geomorphology;
ii) The Dynamic model: Driven by large-scale climate variability, lake levels continued to rise and fall with similar frequency and amplitude to transgressions and regressions that occurred

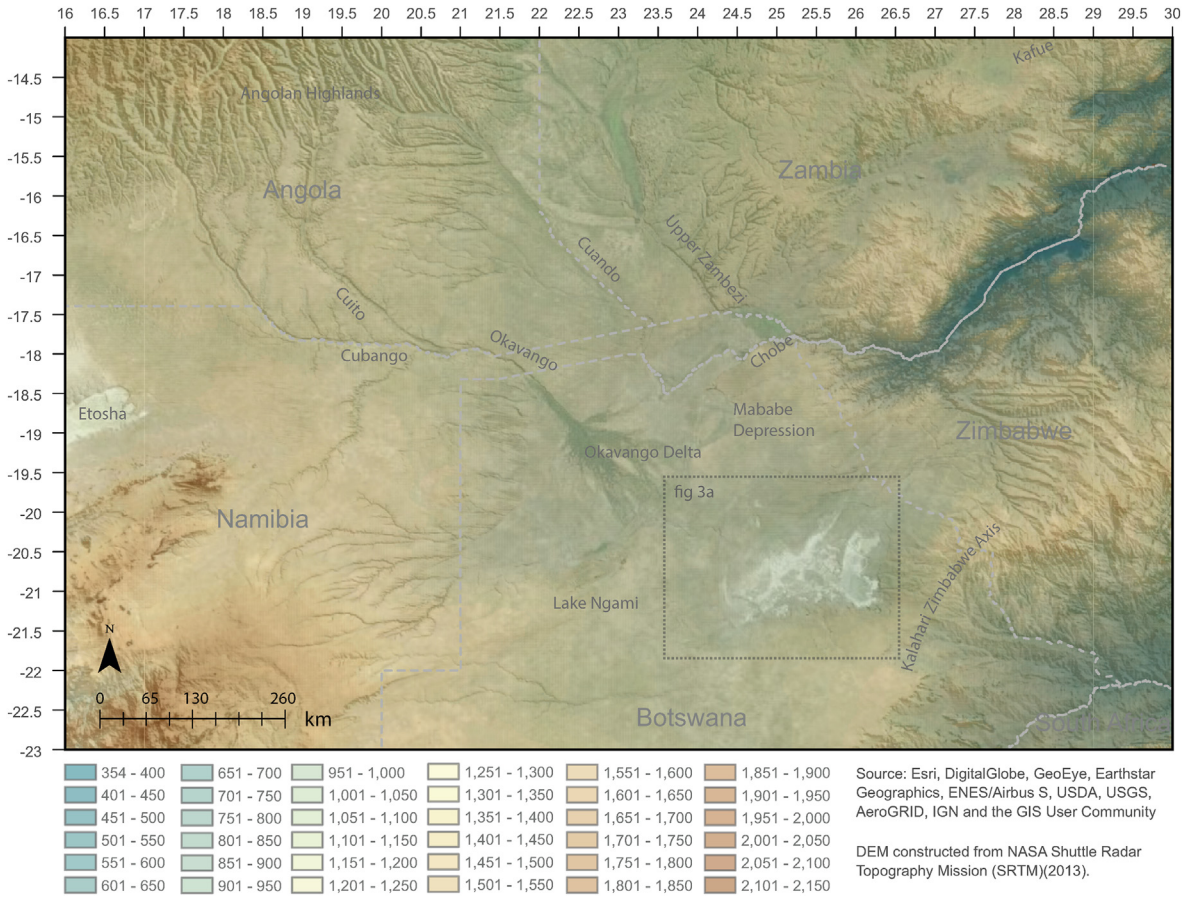

Fig. 1. Digital terrain model of the present-day Makgadikgadi region, its fluvial systems and major geological features.

elsewhere across Africa (e.g. Armitage et al., 2015; Drake et al., 2018; Moernaut et al., 2010; Scholz et al., 2011).

These two divergent and mutually incompatible palaeohydrological models have important implications, not only for our understanding of the mechanisms of late Quaternary hydroclimate change, but for the theories and hypotheses put forward to explain the occupation and dispersal of humans within the interior of Africa during this time. For example, despite strong criticism (e.g. Schlebusch et al., 2021), Chan et al. (2019) invoke the 'push scenario' of a quiescent drying basin after 110 ka as explanation for the outmigration of human populations observed within mitochondrial DNA data.

The Quiescent Model*:* Several researchers (e.g. McFarlane and Eckardt, 2006; Moore et al., 2012) not unreasonably suggest that following the reorganization of fluvial inflow systems, Makgadikgadi effectively dried up in the mid-Pleistocene leaving an exposed basin floor that was dry or seasonally dry and, by comparison to the Pliocene and early Pleistocene, was hydrologically inactive during the late Quaternary and Holocene. Evidence cited to support this idea comes from in-situ surface archaeology, namely artefacts assigned to the Early Stone Age (ESA) on the floor of the 945 m asl Palaeolake Magkadikgadi configuration, 6 km north of Gweta (McFarlane and Segadika, 2001), and at Ngcaezini Pan, 18 km north of Gweta (Robbins and Murphy, 1998) between the 945 and 920 m elevation palaeo-lake shorelines. The implication is that the basin must have been dry since the ESA, a techno-typological era that ended elsewhere in southern Africa ~300 kyrs ago (Wurz, 2020). Similarly, Grove (1969), whose work identified and mapped the shorelines of the palaeolake system, suggested high-lake stands must have pre-dated the Middle Stone Age (MSA) deposits that had been identified by Bond and Summers (1954) on the Nata River that feeds into Sua Pan in the east (Fig. 3a). Since Grove's work, other MSA sites have been recorded right across the Makgadikgadi basin (e.g. Ebert, 1979; Ebert and Hitchcock, 1978; Hitchcock, 1982; Robbins, 1987; Van Waarden, 2010). While both the ESA and MSA material in the basin have no established chronology, the implication of their presence on the lakebed as in-situ sites (i.e. the material has not been washed into the basin from the shorelines) is that a period of hydrological quiescence has prevailed since these artefacts were deposited.

The Dynamic Model*:* In contrast, a growing body of geochronological data, particularly from depositional beach ridges at the margins of the Makgadikgadi basin and from diatom deposits found within the palaeolake, suggest that high lake stands recurred periodically during the last 250 ka (Burrough et al., 2009; Cooke and Verstappen, 1984; Schmidt et al., 2017; Shaw et al., 1997). These large shorelines and thick diatom sequences provide evidence of a lacustrine system with very different hydrological conditions than those of today. At its maximum, it is suggested that the areal extent of this late Quaternary 'megalake system' (Burrough et al., 2009) covered at least 66,000 km^2 (White and Eckardt, 2006) and that it achieved this extent on multiple occasions within the last 200 kyrs. Speculatively, this model invokes a significant inflow contribution from the Zambezi via ponding up of water at the Mambova rapids (at the Zambezi-Chobe confluence) when discharge is extremely high. Back-flow into the palaeolake system would then have occurred via the extremely low gradient Chobe (Burrough and Thomas, 2008; Shaw and Thomas, 1988, 1996; Thomas and Shaw, 1992). Importantly, however, at least some

part of this late Quaternary hydrological dynamism in the Makgadikgadi river catchments is proposed to have occurred in response to high amplitude climate changes occurring both during and after the MSA period, radically modifying the regional and continental landscape and impacting lake levels across Africa (see De Cort et al., 2021).

These two opposing views have come to influence interpretations of an array of geomorphological features within the basin. One of the most well-known and lively of these debates centres on the origin of the enigmatic 'islands' within Makgadikgadi; these are crescentic, vegetated deposits of unconsolidated sand standing several metres above the saline lake floor (Fig. 2). These elevated landforms are characteristically vegetated by only a small number of species, predominantly the grasses *Sporobolus iocladus*, *Sporobolus spicatus* and *Odyssea paucinervis*, that are highly adapted to the saline conditions of the pan (Perkins et al., 2010). The significance of these dune 'islands' in this research arises because of their relationship with well-preserved archaeological material surveyed across a wide area of the lake basin floor. All six of the sites excavated in this study are proximal to these landforms. Despite speculation that the islands were either spring mounds (McFarlane and Long, 2015), shoreline remnants (Franchi et al., 2020), or barchan dunes (Grove, 1969; Burrough et al., 2012; Burrough and Thomas, 2013), a comprehensive study by Richards et al. (2021) convincingly suggests that the processes responsible for these vegetated forms are more closely aligned to those of nebkha dunes. Using a coupled vegetation, sediment transport model, Richards et al. (2021) show that aeolian dunes with a range of morphologies (from crescentic to elongate) are able to form under conditions of uneven surface moisture on the lakebed ("the sticky mound hypothesis").

This study uses both archaeological findings and data on the timing of landform evolution to i) inform the debate on lacustrine activity during the late Quaternary; ii) to establish a chronology for MSA material investigated on pan floor archaeological sites and iii) to examine the influence of landform processes on the potential preservation and visibility of in-situ archaeological material within the basin.

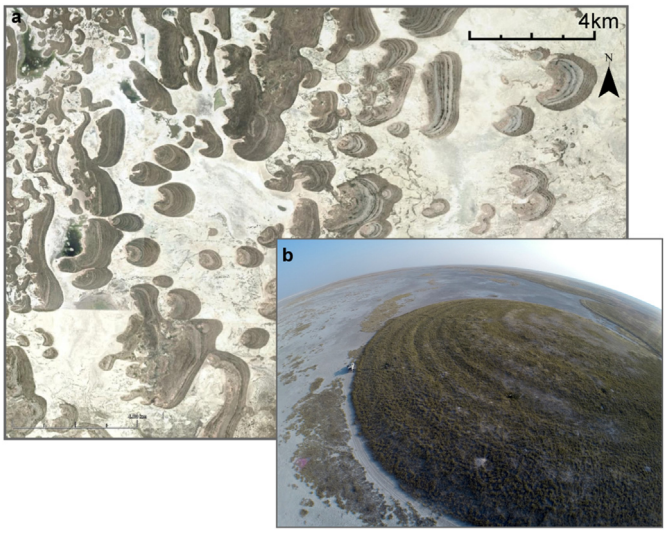

Fig. 2. a) CNES/Airbus Image 2016 (accessible via Google Earth, 2018) of dunes in Ntwetwe Pan (location of image shown in Fig. 1b); b) Drone image of 'island' showing concentric ridging within dunes thought to be caused by decadal/centennial scale accumulations of aeolian sediment (Richards et al., 2021). Figure modified from Burrough, (2022).

3. Methods and sites

3.1. OSL sampling at archaeological sites and surrounds

Stone Age archaeological material is widely distributed throughout the Makgadikgadi basin (Burrough, 2016; Coulson et al., 2022). Following reconnaissance archaeological surveys in the basin in 2008, 2009, 2016 and 2017, six sites on the pan floor (five MSA and one Later Stone Age (LSA)) where well-preserved archaeological material was identified at the surface, were selected for further investigation (Staurset et al., 2022a,b). At each of the archaeological sites, the *décapage* technique was used to carefully remove and sieve sediments in and on which archaeological material was located. After precision mapping of the surface archaeological distributions at each site within quadrants of 1-m grids, the archaeological material was removed and stored at the National Museum of Botswana where *chaîne opératoire* analysis was undertaken with a focus on refitting of artefacts (Staurset et al., 2022b). As the archaeological material from each site was lifted, related sediment samples were taken for Optically Stimulated Luminescence (OSL) dating to enable a timeline for the evolution of the local landscape to be developed. Samples selected for dating included i) Proximal sand dunes; ii) Lakebed sediment directly underlying archaeological material; iii) Lakebed sediment underlying sand dunes; iv) Prominent sand ridges close to archaeological sites (Fig. 3b–e). Samples were extracted in the field either by sectioning and trenching or, where this was not possible, by using a hand-operated hydraulic auger to drill vertically into landforms.

3.2. Site descriptions

Brief site descriptions are provided below where OSL data was also present and the relationship of sampled sites to investigated archaeological sites is detailed in Table 1. Archaeological sites are identified using prefix MAK followed by a number and, if the area contains distinct sub-sites, a letter (e.g. MAK14K). OSL sampling locations associated with these sites are identified using the prefix MAK/followed by the sampling year, archaeological site number, sample site number and the individual sample number within that site number (e.g. MAK/16/14K/1/2, where 16 = 2016, 14 K = archaeological site, 1 = OSL sample site at that location, and 2 = individual sample number).

3.2.1. Ntwetwe Central

Sites in this part of Ntwetwe Pan (Fig. 3a, b, c) were located on or close to the main cutline (a firebreak used as a track) that provides N–S access through the pan. Further description of finds and excavation procedure can be found in Staurset et al., (2022a).

3.2.1.1. Archaeological site MAK15. The archaeological site at MAK15 (Fig. 3b) was limited in size (<25 m^2 excavated) lying along the main track through the pan and adjacent to a morphologically-indistinct lakebed dune to the south (elevated, vegetated zones of sandy deposits). Archaeological material was found on the surface, with the exception of a single artefact that was recovered within a 1 m sample trench (see section 2), at the same level as the remainder of the lithic assemblage. Samples for OSL dating were taken from above and below this level.

3.2.1.2. Archaeological sites MAK14K and MAK14O. The archaeological area of MAK14 extends over c.250 × 600 m and contains 15 archaeological sites and scatters, of which two, MAK14K and MAK14O, were excavated (Figs. 3c and 4). MAK14K comprised 88 artefacts located on the surface of the 42 m^2 excavated area and its immediate surrounds and MAK14O comprised 100 m^2, twice the

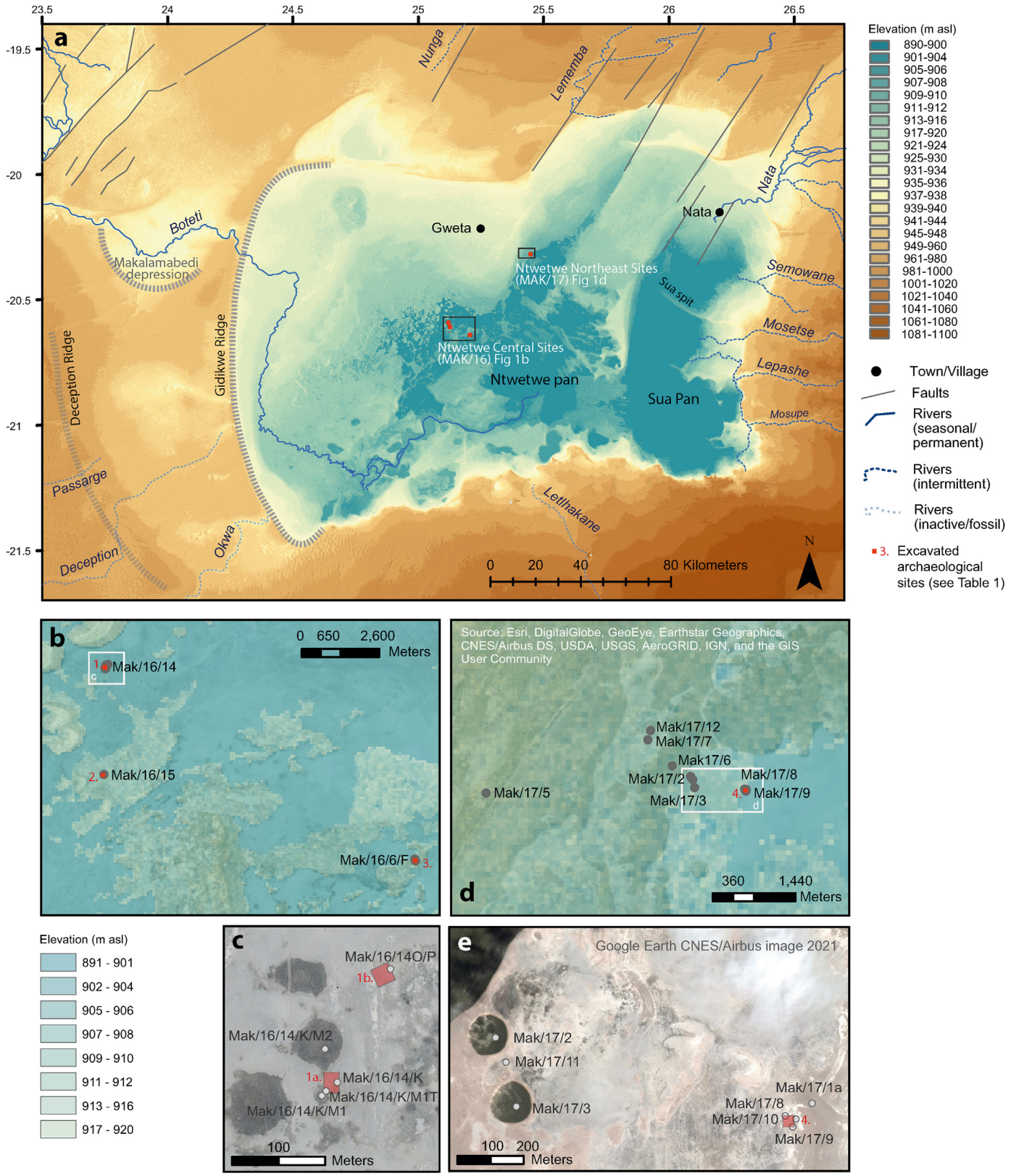

Fig. 3. a) Digital Elevation Model of the Makgadikgadi basin and its major features. The location of dated sites associated with archaeological excavations in Ntwetwe Central (b) and Ntwetwe Northeast (c) and specific site locations are shown in greater detail in the Google Earth imagery of d and e respectively. Details of archaeological sites 1–4 can be found in Table 1.

Table 1
Sample site locations and landforms associated with or proximal to excavated archaeological sites. See Fig. 3 for location of archaeological and OSL sites.

Location	Proximal Archaeological site	OSL sample site ID	Description
Ntwetwe Central	1. Area MAK14 (Including sites 1a MAK14K and 1 b MAK14O)	MAK/16/14 K	Pit into lakebed sediments below archaeological site.
		MAK/16/14K/M1T	Trench running from archaeological site into dune M1.
		MAK/16/14K/M1	Augur hole into the dune M1 located just south of the archaeological site capturing both dune sediments and lakebed material (MAK/16/14K/M1/3) below the dune
		MAK/16/14K/M2	Augur hole into the dune M2 located just north of the archaeological site.
		MAK/16/14O	Pit into lakebed sediments within excavation area MAK14O
	2. MAK15	MAK/16/15	Trench through dune adjacent to MAK15
	3. MAK6	MAK/16/6/F1	Trench into base of Gabasadi Island dune on its western side proximal to LSA material finds at MAK6. The site was considered disturbed.
		MAK/16/6/F2	Trench within dune sediments of Gabasadi Island proximal to LSA material finds at MAK6
Ntwetwe Northeast	4. MAK33	MAK/17/8	Pit into lakebed sediments 3 m northeast of main excavation area within archaeological site MAK33
		MAK/17/9	Pit into lakebed sediments 5 m south of main excavation area within archaeological site MAK33
		MAK/17/10	Pit into lakebed sediments 3 m east of main excavation area within archaeological site MAK33.
		MAK/17/1a	Vibracore sample 80 m northeast of archaeological site MAK33.
		MAK/17/2	Augur hole into dune 900 m to the northwest of MAK33 capturing both dune sediments and lakebed material (MAK/17/2/3) below the dune.
		MAK/17/3	Augur hole into dune 780 m to the west of MAK33 capturing both dune sediments and lakebed material (MAK/17/3/4 and MAK/17/3/5) below the dune.
		MAK/17/11	Pit into lakebed sediment between dunes D2 and D3.
		MAK/17/5	Augur hole into Vegetated ridge 4.2 km to the west of MAK33
		MAK/17/6	Augur hole into elongated dune D6 1.26 km to the northwest of MAK33
		MAK/17/7	Augur hole into dune D7 within pan floor margin area.
		MAK/17/12	Pit into lakebed proximal to dune D7

area of MAK14K and with an assemblage six times larger. The former lies adjacent to two small, vegetated dunes, M1 and M2, c.15 and 50 m in diameter respectively (Fig. 4). The latter lies approximately 150 m to the northeast, adjacent to a prominent N–S band of hardened clay on the lakebed surface. To establish a chronology for the archaeology and to understand the evolution of the landscape at this site, samples for OSL dating were extracted from a pit dug within the archaeological site to capture near-surface and deeper sediments immediately under the artefact layer and additionally from proximal sand dunes and a trench that extended from the MAK14K site back into the M1 dune.

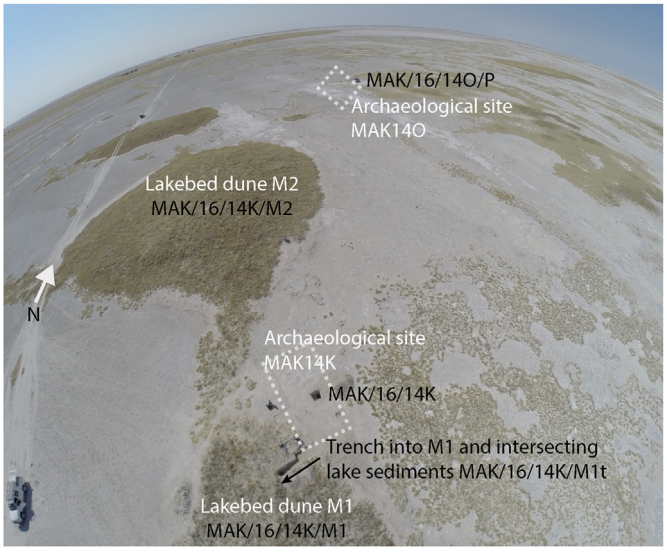

Fig. 4. Drone image, looking north, of archaeological area MAK14 (Ntwetwe Central) including sites MAK14K and MAK14O. OSL sample sites in associated landforms are also shown in black (see Table 1). Note the site sizes are not to scale in this image.

3.2.2. Ntwetwe Northeast

Archaeological site MAK33 is located in the northeastern fault-controlled spur of Ntwetwe Pan, approximately 5 km from an elevated ridge (918 m asl) that forms part of the western shorezone (Fig. 3a,d,e). The excavated area is demarcated by sample pits MAK/17/8, MAK/17/9 and MAK/17/10. The area is impacted, to an unknown degree, by neo-tectonism. The pan margin ridge (location of site MAK/17/5) lies parallel to a horst and graben structure expressed further to the north (Eckardt et al., 2016). Between the ridge and the excavation site lies a messy zone of elongated dunes running parallel to the pan margin with some evidence that overland surface flow previously debouched on to the pan floor (Fig. 3d). The pan floor is visible between the dunes and the ridge (Fig. 5). The impact of faulting here has also caused this area to periodically receive overland or subsurface flow even during relatively dry times, evident by gravelly sediments deposited in shallow channels through the lakebed dunes and on to the pan floor. Permanent water is today found at seepage points a few km to the southwest and northwest of MAK33 (McCulloch et al., 2010).

3.2.2.1. Archaeological site MAK33. The excavated area of the archaeological site covered 430 m^2 across the present-day pan floor on a former swash zone that lies at a more elevated position (~908 m asl) relative to the central and western part of the pan floor in the Ntwetwe spur (904–906 m asl) (Fig. 5). The surface sediments are made up of weakly silica-cemented sands, silt and clay. The site lies a few hundred metres from dunes to the west (MAK/17/2 and MAK/17/3) and overlies a crescentic area of sediments that

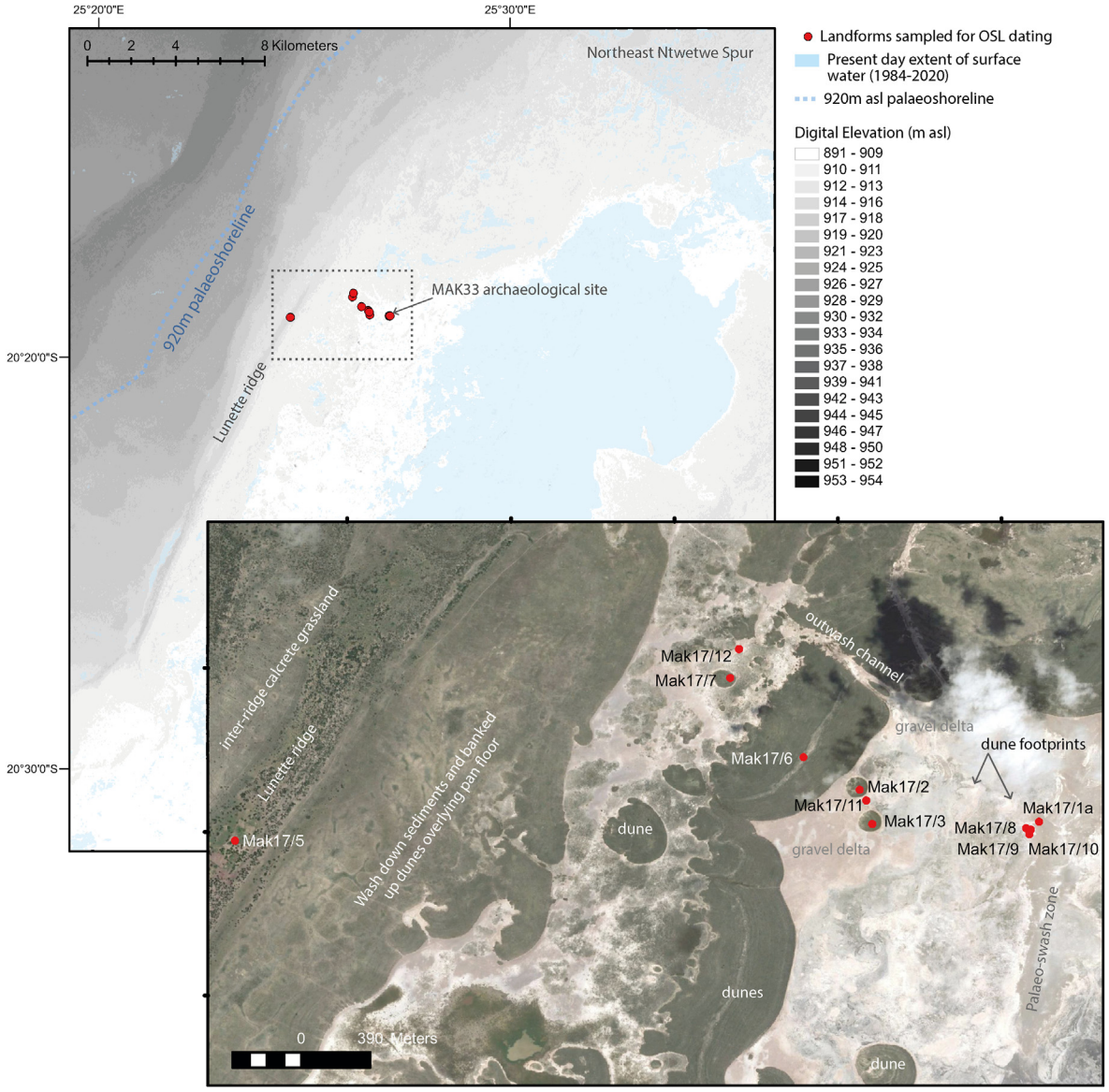

Fig. 5. Digital elevation model and Google Earth imagery (inset) of the Ntwetwe Northeast sites from the western ridge east to the pan floor through the archaeological site MAK33 (location of inset marked by dotted line on the digital elevation map).

could represent the 'footprint' of a former lakebed dune. Landsat imagery suggests standing water (or a shallow seasonal lake) has been present in this part of the pan 2.5 km to the east on numerous occasions. Given its proximity to the present-day pan floor margin 2.5 km to the west, sediments of this part of the basin floor are complex to interpret. There is strong overprinting by ephemeral evaporites, as well as wash-down sediments from the ridge that runs parallel to the pan edge and from inflow from the north of the basin, creating small, coarse sediment (including gravel) deltas and basin edge deposits on the pan floor. Pits were dug to the west (MAK/17/10), east (MAK/17/8) and south (MAK/17/9) of the excavation. The weakly silicified nature of the sediment limited the pit depths to 0.4, 0.5 and 0.3 m respectively. Sediments within the pits consisted of laminated sands, silts and clays with intermittent layers of green-black cal-silcrete fragments up to 8 cm across (see section 4.3). Site MAK/17/8 also contained a trace fossil of a root within a layer containing cal-silcrete fragments at 0.25 m depth. No further analysis was undertaken on the root fossil.

3.2.2.2. Ridge running parallel to the northern fault-controlled spur of Ntwetwe Pan MAK/17/5. A narrow, distinct, ridge stands 14 m above the present-day lakebed floor as part of the basin margin complex, and extends from just a few km NE of the excavation in a SSW direction for ~54 km, parallel to the 920 m palaeolake shoreline before curving round the southern headland into central Ntwetwe (Fig. 5). It is composed of unconsolidated sands and silts and covered by *Digitaria-Antephora* grasslands scattered with mature trees (including *Acacia, Terminalia* and *Commiphora*); scatters of silcrete cobbles occur at various points along the base of the ridge suggesting that the underlying sediment may be silicified. The ridge sustains a handful of cattle posts and numerous domestic stock, particularly cattle and horses, which access groundwater via

deep boreholes. The ridge is underpinned by low-displacement horst and graben structures (Eckardt et al., 2016) but prevailing winds from the east support sediment accumulation either through aeolian (e.g. lunette) or lacustrine processes (i.e. beach ridge), though deposition through both these processes are not mutually exclusive, *senso* Burrough and Thomas (2009). The partially vegetated area immediately east of the ridge was formerly part of the main Ntwetwe spur pan floor, which extended further west towards the 920 m shoreline. Heavily disturbed MSA material has been observed both in this marginal zone and within the calcretised low-lying area between the ridge and the 920 m shoreline to the west.

3.2.2.3. Lakebed dunes and underlying sediments proximal to MAK33. Small dunes lie ~780 m west of the main excavation and rise only 1.5–1.6 m above the lakebed floor at 910–914 m asl. They stand out prominently from the pan surface in remotely sensed imagery due to their vegetated surfaces of saline adapted grasses (e.g. Fig. 3e). The dunes are either small (~100 m in diameter) and distinctly crescentic in shape (MAK/17/2, MAK/17/3, MAK/17/7) or broad, elongate features (MAK/17/6) that parallel the shoreline. Concentric ridging, probably caused by seasonal or decadal accumulation of sediments (Richards et al., 2021) is visible remotely. These dunes were sampled using a handheld auger.

3.3. Sedimentology

From each sample, 10–20 g of material was subsampled to examine the sediment grain size distribution. Particle size analysis (2–2000 μm grains) was carried out using a Malvern Laser Particle Size Analyser (Hydro, 2000MU) and sediment statistics calculated using the Folk and Ward formulae (Folk and Ward, 1957).

3.4. Geochronology

The depositional age of the sediment, collected in opaque plastic tubes, was determined using OSL dating at the Oxford Luminescence Dating Laboratory. Sample preparation was carried out under subdued red light (600 nm) conditions and the outer light-contaminated material was removed and later sub-sampled for dosimetry and sedimentology. Quartz grains used to determine equivalent doses (D_e) were isolated from the remaining sediment bulk using 37% HCl and 30% H_2O_2 to eliminate carbonates and organics respectively. The 180–212 μm fraction was separated by wet-sieving. Density separation using sodium polytungstate was used to partition quartz (>2.62 and < 2.7 gcm^{-3}) from feldspars and heavy minerals. The quartz separate was then treated with 40% HF for 50 min to remove the α-irradiated outer surface and any remaining feldspar component. This was followed by a 24-h HCl wash to remove fluorides and then back-sieved using a 180 μm sieve mesh. The remaining 180–212 μm quartz grains were mounted on to either i) aluminium discs using a 2 mm diameter mask and silicon oil spray for multigrain analysis or ii) into an array of a hundred 300-μm holes in the surface of an aluminium disc for single grain analysis. In addition, as the silt content of lakebed samples was, on average, higher than that in subaerial features, the fine grain fraction (4–11 μm) was also used to determine ages for some samples. Following pre-treatment with HCl and H_2O_2 as above, these samples were then settled using Stoke's law to separate the 4–11 μm grains. They were then left in Fluorosilic acid (H_2SiF_6) for 10 days to remove feldspars prior to a final HCl wash and were subsequently mounted in a monolayer on aluminium discs.

3.4.1. Equivalent dose (De) determination

Multi-grain preheat plateau and range-finder tests were carried out for a selection of samples from each location. Single grain D_e determination was undertaken on 500–3000 individual quartz grains for each sample, from which there was an average useable signal yield of 7%. The D_e for each grain was measured using single-aliquot regenerative-dose (SAR) protocol (Murray and Wintle, 2003). The distribution of D_e measurements from single-grain analyses is advantageous primarily because it provides a D_e distribution that allows a much clearer assessment of depositional and/or post-depositional processes, critical for informing the choice of age model used to produce the final age. For very young samples however, the OSL signals were particularly dim and low-yielding (with less than 1% grains giving a measurable signal). For these sediments, multigrain measurements were instead used to determine the D_e.

3.4.2. OSL measurement conditions and rejection criteria

We used a TL-DA-15 reader with an EMI9235QA photomultiplier fitted with two 3 mm thick U-340 filters. Laboratory radiation doses were given by exposure to a $^{90}Sr/^{90}Y$ beta source calibrated for each grain position within a single disc. Preheats were chosen following preheat plateau tests that indicated relatively little systematic dependency on preheat in older samples (PH1 = 260/240 °C, 10 s and PH2 = 220 °C, 0 s) but much better performance at lower temperatures for younger samples (PH1 = 200 °C, 10 s and PH2 = 180 °C, 0 s). OSL measurements were made using a focused 532 nm laser for 1 s of stimulation with data recorded in 60 channels. Luminescence signals were integrated using the first five channels (0.1s) to maximise fast component dominance and minimise any possible unstable medium component contamination. Instrumental noise was measured using a background subtraction of the last 20 channels (0.4s) of the OSL decay. Sensitivity corrections were monitored using recycled laboratory dose responses and potential feldspar contamination was assessed using IR-OSL depletion ratios (Duller, 2003). In both cases aliquots were rejected if these ratios lay outside 30% of unity with average recycling and IR depletion ratios being 1.03 and 0.99 respectively. Additionally, grains were also rejected if the test dose signal (Tn) was dim (if the initial Tn signal was less than 3σ above the corresponding background count). Thermal transfer was monitored by measuring the OSL response of each quartz grain to a 'zero dose' irradiation, expressed as a percentage of the natural signal. Grains were rejected for potential transfer of charge during SAR if this measurement exceeded 5 or 20% of the natural signal for older/very young samples respectively (the higher value for younger samples takes account of the absolute recuperated charge remaining constant but increasing as a proportion of the smaller D_e values). We assumed a 2.5% uncertainty for measurement reproducibility (Thomsen et al., 2005). A dose recovery test (DRT) at the expected D_e value (determined using the initial range finder test) was undertaken for 1–3 samples from each site location providing an average recovery ratio of 0.97 ± 0.2 (Fig. 6a).

For older samples, where the intersection of the natural dose with the dose response curve approached the asymptote (D_0) of the exponential fit, i.e. some grains or aliquots were near to saturation, we applied an additional selection criteria to mitigate against possible saturation effects on the sample. For these samples the D_e

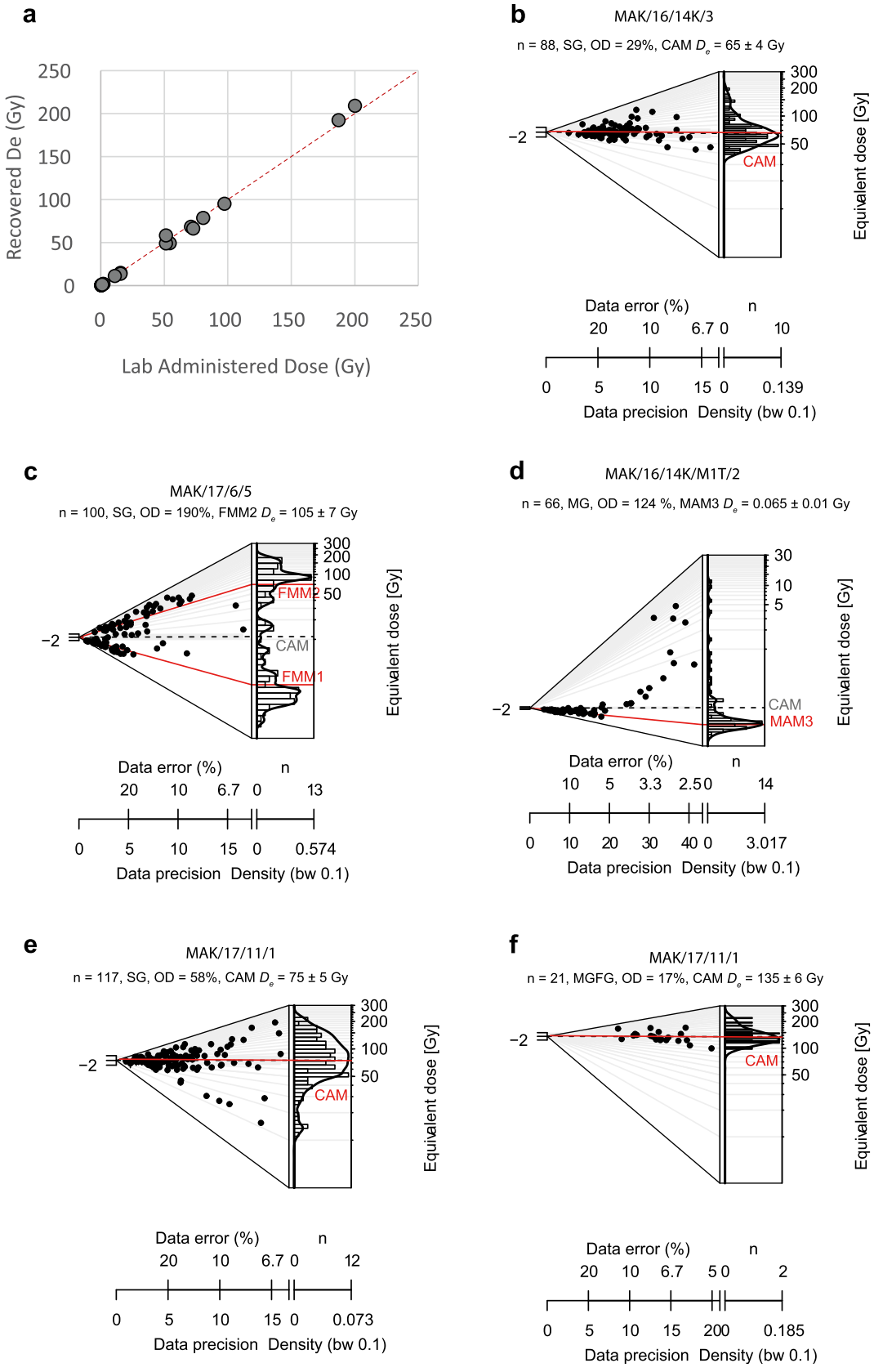

Fig. 6. a) Dose recovery tests using quartz OSL SAR protocol for a subset of samples investigated in this study b-e) Example D_e distributions for b) Single Grain (SG) distribution where age was determined using the CAM model; c) Bimodal SG distribution where the finite mixture model (FMM) was used to determine age; d) Multigrain D_e distribution where the Minimum Age model (MAM3) was used to determine age; e) SG distribution where 37% of measured signals were saturated; f) Multigrain fine grain measurements for the same sample (8% of measured signals were saturated).

was iteratively calculated using a progressively more stringent D_0 threshold applied in 10 Gy increments (e.g Thomsen et al., 2016; Guo et al., 2017). Where a rise to a plateau was observed, the lowest D_0 threshold included in the plateau was used to select the appropriate D_e (Fig. S1 in the Supplementary Material). This was typically when the D_0 threshold was between 30 and 80 Gy (Table S1). Many samples exhibited falling or stable plateaus with increasing D_0 thresholds. In these cases, D_0 threshold = 0 was appropriate and the D_e was calculated using all grains or aliquots resulting in no change to the calculated age with the application of this criteria.

3.4.3. Dose rate (D') determination

The dose rate for OSL age calculation was determined using Inductively Coupled Plasma Mass Spectrometry (ICP-MS) to measure isotope concentrations (^{232}Th, ^{238}U and ^{4} K) within the sample. Dose rate calculations were undertaken in Excel. Conversion to external beta and gamma components (to account for grain-size, HF etching and moisture content) used the dose-rate conversion and beta attenuation factors of Guérin et al. (2011); Guérin et al. (2012) and Mejdahl (1979), assuming radioactive equilibrium in the ^{238}U and ^{232}Th series. Gamma dose was adjusted where samples lay close to the surface (Aitken, 1985) to account for the inert atmosphere above ground level though we note that this may not have always been the case during burial. Sample moisture contents during burial were estimated at 10 ± 5% for sand mounds and ridges and 15% for lakebed material which contained more finer-grained sediment and which lay closer to the fluctuating water table. Cosmic-ray dose was calculated according to Prescott and Hutton (1994).

3.4.4. Age model selection

The challenge for establishing a robust geochronology is that many of the depositional ages for sediments in this study lie at either the lower or upper limit of OSL dating. The choice of age model was affected by the grain-size used and the characteristics of the D_e distribution including the potential for signal saturation.

I) *Coarse, single grain quartz ages*: Ages from equivalent doses generated from single grains of quartz, where there was no discernible evidence for biological mixing or sample saturation, were calculated using the central age model (CAM) (Fig. 6b). Three samples exhibited distinct bimodal populations (e.g. Fig. 6c) and in each case there was visible evidence within the sediment of having sampled across sedimentological breaks that represented a chronostratigraphic boundary. For these samples the Finite Mixture Model (FMM) was used to extract multiple age components from the distribution. The optimum number of FMM components was selected taking into consideration the Bayesian Information Criterion and log likelihood statistical parameters. The representative component was then chosen taking into consideration the section stratigraphy and the proportion of grains within each age group. Phantom groups or groups containing only one or two grains were not

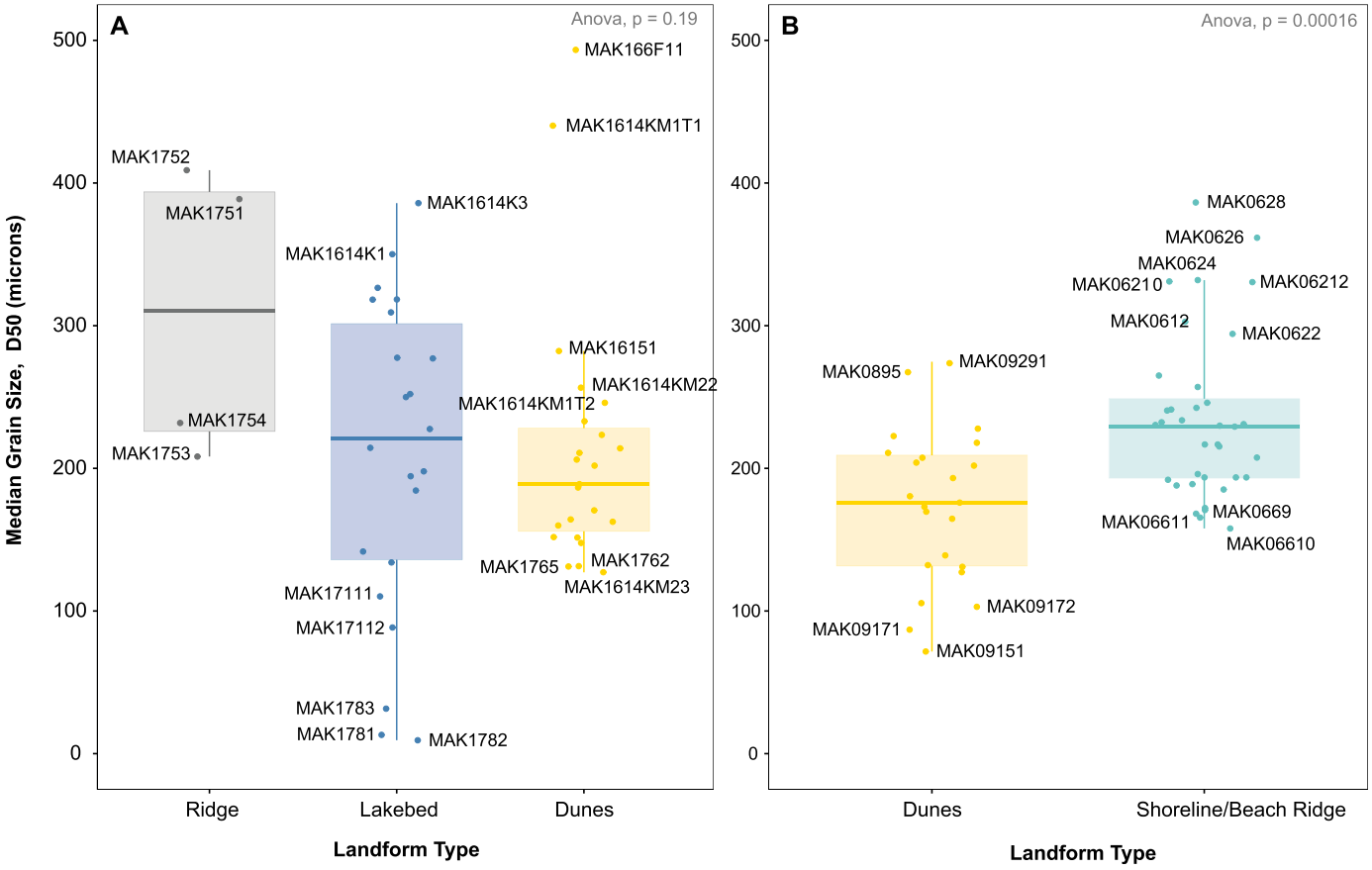

Fig. 7. Median grainsize values for landform types in the Makgadikgadi for A) this study and B) previous studies (Burrough et al., 2009, 2012). Samples with median grainsizes at the outer limits of the grainsize distribution for each landform type are labelled with their sample ID.

Table 2
Grainsize characteristics for dated samples.

Sample	Landform	% Content by Volume										
		Clay	Silt	VF Sand	F Sand	M Sand	C Sand	VC Sand	D50	MEAN	MODE1	SORTING
MAK/16/14K/1	lakebed	0	2	3	23	50	22	0	350	381	386	0.79
MAK/16/14K/2	lakebed	0	2	7	28	43	20	0	318	359	386	0.92
MAK/16/14K/3	lakebed	0	3	2	17	52	27	0	386	415	436	0.78
MAK/16/15/1	dune	0	3	5	34	44	13	1	282	329	302	0.84
MAK/16/15/2	lakebed	1	11	8	31	40	10	0	252	278	302	1.29
MAK/16/15/3	lakebed	0	7	6	30	42	13	1	278	321	302	1.11
MAK/16/6/F1/1	dune	0	3	3	13	34	35	12	493	581	556	1.12
MAK/16/6/F2/1	dune	3	23	14	22	24	11	2	171	259	302	2.05
MAK/16/6/F2/2	dune	3	21	12	21	27	14	2	202	278	341	2.06
MAK/16/14K/M1T/1	dune	1	4	4	17	34	31	10	440	531	492	1.21
MAK/16/14K/M1T/2	dune	2	6	8	35	38	10	1	246	286	267	1.22
MAK/16/14K/M1T/3	lakebed	7	30	9	20	24	9	1	142	212	302	2.45
MAK/16/14K/M1T/4	lakebed	5	25	8	22	29	10	2	198	255	302	2.30
MAK/16/14K/M1T/5	lakebed	3	16	5	26	39	11	0	250	272	302	1.83
MAK/16/14O/1	lakebed	3	15	3	23	43	13	0	277	292	341	1.81
MAK/16/14O/2	lakebed	1	6	1	23	53	17	0	327	351	341	1.01
MAK/16/14K/M1/1	dune	4	14	16	41	23	2	0	163	181	185	1.54
MAK/16/14K/M1/2	dune	4	18	7	24	33	13	0	233	270	341	2.09
MAK/16/14K/M1/3	lakebed	5	14	3	17	43	18	0	309	323	386	2.09
MAK/16/14K/M2/1	dune	2	8	9	38	35	7	0	223	253	237	1.36
MAK/16/14K/M2/2	dune	2	8	4	34	43	8	0	257	277	267	1.25
MAK/16/14K/M2/3	dune	9	30	9	18	23	10	0	127	201	341	2.61
MAK/16/14K/M2/4	lakebed	5	18	3	13	41	21	0	318	326	436	2.24
MAK/17/2/1	dune	0	3	24	31	25	13	4	214	234	164	1.13
MAK/17/2/2	dune	3	14	20	24	23	14	2	187	178	145	1.86
MAK/17/2/3	lakebed	5	18	15	16	17	18	13	228	200	906	2.42
MAK/17/3/1	dune	0	7	22	29	26	14	2	211	221	164	1.28
MAK/17/3/2	dune	1	5	24	36	26	7	1	189	194	164	1.19
MAK/17/3/3	dune	4	17	21	22	19	13	3	164	133	145	2.18
MAK/17/3/4	lakebed	4	25	21	20	16	11	3	134	114	145	2.21
MAK/17/5/1	ridge	1	9	5	15	36	28	6	389	350	436	1.47
MAK/17/5/2	ridge	1	3	9	22	24	29	12	409	394	710	1.26
MAK/17/5/3	ridge	3	14	18	23	25	15	3	208	196	185	1.76
MAK/17/5/4	ridge	2	10	18	23	26	18	3	232	230	185	1.58
MAK/17/6/1	dune	0	7	31	40	18	2	1	160	159	164	0.89
MAK/17/6/2	dune	1	9	42	35	8	3	1	131	131	129	1.02
MAK/17/6/3	dune	2	8	35	36	14	5	1	148	151	145	1.20
MAK/17/6/4	dune	0	3	37	47	11	1	1	152	152	145	0.63
MAK/17/6/5	dune	7	19	25	25	14	8	1	132	87	145	2.32
MAK/17/7/1	dune	4	17	24	24	16	11	4	151	137	145	2.10
MAK/17/7/2	dune	2	9	21	26	20	17	6	206	232	145	1.67
MAK/17/8/1	lakebed	24	54	9	6	4	2	1	13	16	9	2.49
MAK/17/8/2	lakebed	28	67	5	1	0	0	0	9	9	10	1.83
MAK/17/8/3	lakebed	13	53	18	10	5	1	0	32	29	101	2.27
MAK/17/9/1	lakebed	3	10	22	28	21	12	3	185	194	164	1.66
MAK/17/9/2	lakebed	3	9	22	28	23	13	2	194	205	164	1.57
MAK/17/10/1	lakebed	4	10	19	23	23	17	5	214	218	164	1.87
MAK/17/11/1	lakebed	6	30	20	19	15	7	2	110	85	145	2.31
MAK/17/11/2	lakebed	6	37	21	18	9	5	3	88	64	129	2.32

considered to be robust and in each case the component that made most sense in terms of the section stratigraphy also contained the greatest proportion of grains. Where possible, where coarse grain D_e distributions contained more than 10% saturated signals, we also measured the fine grain component (4–11 μm), which exhibited higher dose saturation characteristics compared to the coarse grain component.

II) *Coarse, multigrain quartz ages*: Sediments from some of the lakebed dunes, mobilised and deposited in the last few hundred years, have OSL signals that are, on the whole, too dim for detection at the single grain scale. Multigrain analysis bulks up these signals to allow a better signal to noise ratio. Measuring many grains at once however, masks anomalous equivalent doses with poor luminescence characteristics, and the inclusion of these grains causes averaging effects that tend to overestimate sample depositional age (Russell and Armitage, 2012). To mitigate against this effect and minimise any age overestimate, we have used the 3-parameter minimum age model (MAM3) to date these younger samples (Fig. 6d). Strictly, this model should only be used with single grain data (see Arnold et al., 2009) but Richards et al. (2021) showed that, where comparative single grain and multigrain data are available from the basin, multigrain MAM3 ages deviate less from the single grain ages than other age models. Nevertheless, in this comparison, multigrain ages can overestimate single grain ages by up to

Table 3
Dose rate measurements for dated samples.

Sample ID	Depth (m)	Grain size (μm)	% K (±20%)	Th (ppm) (±20%)	U (ppm) (±20%)	Depth (m) (±0.05 cm)	Latitude	Longitude	Altitude (m above sea-level)	Moisture (water/wet sediment)	Total dose rate (Gy/ka) error
MAK/16/14K/M1T/1	0.19	180–210	0.31	2.88	0.74	0.19	−20.586	25.1195	904	10%	0.82 ± 0.10
MAK/16/14K/M1T/2	0.42	180–210	0.36	2.05	0.57	0.42	−20.586	25.1195	904	10%	0.78 ± 0.08
MAK/16/14K/M1T/3	0.58	180–210	0.70	2.75	0.73	0.58	−20.586	25.1195	904	15%	1.09 ± 0.13
MAK/16/14K/M1T/4	0.6	180–210	0.63	2.38	0.68	0.6	−20.586	25.1195	904	15%	1.00 ± 0.12
MAK/16/14K/M1T/5	0.69	180–210	0.42	2.25	0.64	0.69	−20.586	25.1195	904	15%	0.82 ± 0.09
MAK/16/14K/1	0.2	180–210	0.40	1.29	0.35	0.2	−20.586	25.1195	904	10%	0.72 ± 0.10
MAK/16/14K/2	0.5	180–210	0.46	1.75	0.48	0.5	−20.586	25.1195	904	15%	0.79 ± 0.09
MAK/16/14/K/3	0.8	180–210	0.46	1.64	0.44	0.8	−20.586	25.1195	904	15%	0.77 ± 0.09
MAK/16/14K/M1/1	0.8	180–210	0.53	2.76	0.79	0.8	−20.586	25.1193	907	10%	1.01 ± 0.11
MAK/16/14K/M1/2	1.3	180–210	0.43	2.40	0.65	1.3	−20.586	25.1193	907	10%	0.86 ± 0.09
MAK/16/14K/M1/3	2.3	180–210	0.30	1.27	0.39	2.3	−20.586	25.1193	907	15%	0.57 ± 0.06
MAK/16/14K/M2/1	0.8	180–210	0.42	2.18	0.59	0.8	−20.586	25.1194	907	10%	0.83 ± 0.09
MAK/16/14K/M2/2	1.4	180–210	0.40	2.31	0.71	1.4	−20.586	25.1194	907	10%	0.83 ± 0.09
MAK/16/14K/M2/3	2.0	180–210	0.64	3.12	0.80	2	−20.586	25.1194	907	10%	1.10 ± 0.13
MAK/16/14K/M2/4	2.8	180–210	0.26	1.03	0.37	2.8	−20.586	25.1194	907	15%	0.51 ± 0.05
MAK/16/14O/1	0.2	180–210	0.22	1.29	0.40	0.2	−20.585	25.12	904	15%	0.56 ± 0.08
MAK/16/14O/2	0.45	180–210	0.21	1.21	0.49	0.45	−20.585	25.12	904	15%	0.56 ± 0.05
MAK/16/15/1	0.39	180–210	0.40	1.52	0.41	0.39	−20.62	25.12	910	10%	0.76 ± 0.09
MAK/16/15/2	0.60	180–210	1.07	2.54	0.68	0.60	−20.62	25.12	910	15%	1.37 ± 0.19
MAK/16/15/3	0.90	180–210	1.02	2.00	0.53	0.90	−20.62	25.12	910	15%	1.26 ± 0.18
MAK/16/6/F1/1	0.4	180–210	0.76	4.28	1.12	0.4	−20.643	25.2125	909	10%	1.38 ± 0.16
MAK/16/6/F2/1	0.42	180–210	1.08	3.86	1.18	0.42	−20.644	25.2127	911	10%	1.64 ± 0.21
MAK/16/6/F2/2	0.98	180–210	1.15	4.80	1.34	0.98	−20.644	25.2127	911	10%	1.78 ± 0.23
MAK/17/2/1	0.5	180–210	0.59	2.53	0.72	0.5	−20.314	25.4428	910	10%	1.04 ± 0.12
MAK/17/2/2	1.5	180–210	0.56	2.65	0.75	1.5	−20.314	25.4428	910	15%	0.95 ± 0.11
MAK/17/2/3	1.7	180–210	1.35	3.61	1.02	1.7	−20.314	25.4428	910	15%	1.69 ± 0.24
		4–11									1.94 ± 0.27
MAK/17/3/1	0.5	180–210	0.53	3.11	0.99	0.5	−20.316	25.4434	912	10%	1.08 ± 0.12
MAK/17/3/2	1.0	180–210	0.56	2.64	0.73	1	−20.316	25.4434	912	10%	1.01 ± 0.11
MAK/17/3/3	1.3	180–210	0.44	2.89	0.77	1.3	−20.316	25.4434	912	10%	0.92 ± 0.10
MAK/17/3/4	1.65	180–210	0.73	3.05	0.92	1.65	−20.316	25.4434	912	15%	1.14 ± 0.14
MAK/17/3/5	1.8	180–210	0.94	2.96	0.90	1.8	−20.316	25.4434	912	15%	1.30 ± 0.17
		4–11									1.52 ± 0.19
MAK/17/4/1	0.38	180–210	0.53	3.11	0.99	0.38	−21.103	24.6481	915	10%	1.08 ± 0.12
MAK/17/4/2	0.65	180–210	1.14	4.04	1.74	0.65	−21.103	24.6481	915	10%	1.81 ± 0.23
MAK/17/4/3	1.15	180–210	1.17	4.67	1.53	1.15	−21.103	24.6481	915	10%	1.83 ± 0.23
MAK/17/5/1	0.6	180–210	0.27	2.83	0.67	0.6	−20.317	25.411	918	10%	0.78 ± 0.07
MAK/17/5/2	1.1	180–210	0.30	2.63	0.63	1.1	−20.317	25.411	918	10%	0.76 ± 0.07
MAK/17/5/3	2.0	180–210	0.53	3.11	0.93	2	−20.317	25.411	918	10%	1.03 ± 0.11
MAK/17/5/4	3.0	180–210	0.61	3.01	1.16	3	−20.317	25.411	918	15%	1.06 ± 0.12
MAK/17/6/1	0.5	180–210	0.61	1.83	0.85	0.5	−20.313	25.4399	914	10%	1.05 ± 0.12
MAK/17/6/2	1.0	180–210	0.87	2.19	0.70	1	−20.313	25.4399	914	10%	1.25 ± 0.16
MAK/17/6/3	1.5	180–210	0.70	2.08	0.68	1.5	−20.313	25.4399	914	10%	1.08 ± 0.13
MAK/17/6/4	2.0	180–210	0.72	1.60	0.55	2	−20.313	25.4399	914	10%	1.02 ± 0.13
MAK/17/6/5	2.4	180–210	0.92	2.49	0.8	2.4	−20.313	25.4399	914	15%	1.22 0.16
MAK/17/7/1	0.5	180–210	0.55	2.26	0.66	0.5	−20.309	25.4362	912	10%	0.98 ± 0.11
MAK/17/7/2	1.0	180–210	0.48	1.68	0.61	1	−20.309	25.4362	910	10%	0.86 ± 0.10
MAK/17/8/1	0.13	180–210	1.00	2.97	1.22	0.13	−20.316	25.4513	910	15%	1.46 ± 0.14
		4–11									1.68 ± 0.13
MAK/17/8/2	0.35	180–210	1.20	3.11	1.43	0.35	−20.316	25.4513	910	18%	1.60 ± 0.13
		4–11									1.90 ± 0.14
MAK/17/8/3	0.5	180–210	1.07	3.09	1.12	0.5	−20.316	25.4513	910	19%	1.42 ± 0.11
		4–11									1.71 ± 0.12
MAK/17/9/1	0.17	180–210	0.63	2.76	0.83	0.17	−20.317	25.4514	912	15%	1.07 ± 0.10
		4–11									1.24 ± 0.08
MAK/17/9/2	0.24	180–210	0.53	2.70	0.84	0.24	−20.317	25.4514	912	17%	0.96 ± 0.08
		4–11									1.16 ± 0.08
MAK/17/10/1	0.35	180–210	0.50	3.01	0.89	0.35	−20.317	25.4515	911	15%	0.98 ± 0.07
		4–11									1.17 ± 0.08
MAK/17/11/1	0.18	180–210	0.92	2.99	0.99	0.18	−20.315	25.4431	909	15%	1.34 ± 0.12
		4–11									1.56 ± 0.11
MAK/17/11/2	0.4	180–210	0.89	2.85	0.83	0.4	−20.315	25.4431	909	17%	1.24 ± 0.10
		4–11									1.46 ± 0.10
MAK/17/12/1	0.45	180–210	0.94	2.62	0.66	0.45	−20.307	25.4366	910	15%	1.26 ± 0.10
		4–11									1.46 ± 0.11
MAK/17/1a/4	0.04	4–11	0.88	2.48	0.75	0.04	−20.316	25.4519	908	15%	1.34 ± 0.19
MAK/17/1a/40	0.4	4–11	0.87	3.17	1.45	0.4	−20.316	25.4519	908	18%	1.63 ± 0.20
MAK/17/1a/76	0.76	4–11	0.75	3.28	0.97	0.76	−20.3161	25.45192	908	0.18	1.39 ± 0.16

62% (~60 years) in some cases. This may be the impact of recuperated charge on the very small equivalent doses.

III) *Fine, multigrain quartz ages*: Where possible, lakebed samples were dated using fine (4–11 μm) multigrain quartz where (>10,000) grains are averaged per aliquot. The larger number of grains per aliquot significantly improves the precision of the age estimate (e.g. compare the single grain measurements in Fig. 6e to the multigrain equivalent doses in Fig. 6f). However, because the depositional age of these samples lies at the upper limit of quartz OSL dating, where between 33 and 96% of measured equivalent doses fall close to the asymptote of the OSL growth curve (i.e. $D_e > 2D_0$), there is a possibility that ages derived from these equivalent doses may underestimate true age. The application of a D_0 selection criteria mitigates against this effect (section 3.3.2). We use the CAM age model (Fig. 6f) that, whilst potentially weighting the D_e to more precisely known values at the younger end of the D_e distribution, is less likely to accentuate age underestimation than using the MAM3 age model.

Where both multigrain and single grain measurements for lakebed samples were available, we found the single grain D_e estimates to significantly underestimate the multigrain D_e and produce ages that were frequently stratigraphically inconsistent. This effect could be due to a truncated D_e population reflecting the presence of unmeasurable saturated grains. Alternatively, it may indicate a real post-depositional process for lake-bed samples where sand-sized grains are able to penetrate previously deposited material due to the presence of polygonal clay cracking common at a seasonal scale under present-day conditions. For this reason, we have chosen to use the multigrain ages for lakebed samples where possible.

3.4.5. Post IRIR experiments on feldspars

In an attempt to mitigate against hitting the upper limit of quartz OSL dating, we additionally extracted the K-rich feldspar fraction from samples using heavy liquid separation between 2.53 g/cm^3 and 2.58 g/cm^3. Feldspars made up only a maximum of 8% bw of the mineral composition and many samples yielded no feldspars at all. A sample with the most abundant potassium feldspar fraction at the upper limit of OSL dating was selected for experimental post-IR IR measurements, a technique that tends to minimise the deleterious effects of anomalous fading (Thomsen et al., 2008). The age limit of this technique has been shown to far exceed that of quartz (e.g. Buylaert et al., 2012) and is increasingly routinely used as a dating method. Measurement details for these experiments are given in the online Supplementary Information (Table S2).

4. Results

4.1. Sedimentology

Sediment grain size data for the OSL dated samples are presented in Table 1. One-way ANOVA tests were performed to evaluate whether the sediment grainsize characteristics were different between the landform types sampled: lakebed (n = 22); dunes (n = 22); ridge (n = 4). Tukey post-hoc analyses revealed that samples from ridge sediments contained significantly more coarse material (D90) than either dune or lakebed samples (p = 0.016, p = 0.0014), but no other group differences were statistically significant (Fig. 7a, Table 2). This suggests that, within this environment, landforms cannot be discriminated by grainsize alone.

Sediments from the lakebed dunes were relatively tightly clustered, as is common for features formed through aeolian transport, with median grainsizes that fell between 130 and 230 μm. Sediment samples that were taken close to the present-day dune surface, however (i.e. MAK/16/6/F/1/1, MAK16/14K/M1T1), contained a particularly coarse component. Samples from the lakebed itself showed a wide range of sediment characteristics with median grain sizes varying between 9 and 390 μm, though typically falling within with the 130–310 μm range. Ridge samples had two distinct groups: the upper two samples, where the median value was ~400 μm and the lower two samples where the median values were closer to 200 μm. Data for beach ridge and dune samples from previous studies in the Makgadikgadi are shown for comparison (Fig. 7B).

4.2. Geochronology

4.2.1. Post IRIR feldspar experiments

Dose recovery from feldspar signals was promising with an average recovery ratio of 0.99 ± 0.07 for the pIRIR 290 signal but the pIRIR 225 signal underestimated the given dose by 13%. Residual doses following an 8-day bleach in direct sunlight were high for all pIRIR signals ranging between 22.7 and 34.8 Gy (15–23% of the measured D_e for this sample). Under natural conditions, deposition of these lakebed sediments would have occurred sub-aqueously, attenuating the wavelength and intensity of incident light, lengthening the bleaching time further (Berger, 1990) and likely resulting in much higher dose residuals. Using the central age model, K-feldspars for sample MAK/17/8/1 returned an age of 95 ± 12 ka in comparison to the fine grain quartz age estimate of 91 ± 7 ka. As pIRIR K-feldspar ages could not be analysed systematically across all samples and embedded additional uncertainty into the age estimates due to their unknown bleaching rate and high residual-dose retention, we routinely used quartz to estimate sample depositional age. However, the similar sample ages determined using the two methods for this sample provide added confidence in the fine grain quartz OSL ages from the basin despite showing some signs of saturation during single-grain analyses. K-feldspars are uncommon in these sediments and future pIRIR work will require larger volume samples to be collected.

4.2.2. Quartz ages

Sediment ages derived from OSL dating of quartz are reported in Tables 3 and 4 and Figs. 9–10. Where both single grain and multigrain analyses were performed on samples lying close to the limit of quartz saturation, both ages are presented but fine-grained dates have greater stratigraphic consistency and are used in the final interpretations of landscape evolution in section 5. Where more than 10% of measured single grains were saturated, ages should be interpreted with caution as these may underestimate true age and therefore represent a minimum date for lake sediment deposition. Isotope concentrations suggest 232-Th/238-U ratios are close to 3 across the entire sample dataset. This is similar to crustal averages, which implies an undisturbed ratio between parent U (soluble) and Th (insoluble) isotopes, and therefore disequilibrium in the 238-U decay series is unlikely.

Table 4
Equivalent Dose (D_e) and Age data for dated samples. Samples where more than 30% of grains were saturated lie close to the limit of quartz OSL dating are marked by a star (*). Greyed out data were not used in the final age assessments as they were found to be less stratigraphically consistent, perhaps reflecting truncated D_e distributions due to saturation of a large number of grains or due to contamination from later deposits that migrated through polygonal clay cracks (see 3.3.4).

Sample ID	Landform	Method	% saturated grains/aliquots	n (number of grains/aliquots)	D_e (Gy) (Gy)			Overdispersion (%) error (%)			Grain size (um)	Age model	AGE (ka)		error	% error
MAK/16/14K/M1T/1	lakebed dune	MG		41	0.02	±	0.01	85	±	10	180–210	MAM	0.03	±	0.01	47%
MAK/16/14K/M1T/2	lakebed dune	MG		66	0.07	±	0.01	124	±	11	180–210	MAM	0.08	±	0.02	19%
MAK/16/14K/M1T/3	lakebed	SG	6%	51	64.4	±	2.50	6	±	12	180–210	CAM	58.9	±	7.5	13%
MAK/16/14K/M1T/4	lakebed	SG	3%	60	56.9	±	3.85	33	±	7	180–210	CAM	57.0	±	7.8	14%
MAK/16/14K/M1T/5	lakebed	SG	8%	66	68.3	±	3.25	16	±	8	180–210	CAM	83.7	±	9.7	12%
MAK/16/14K/1	lakebed	SG	5%	82	66.9	±	2.60	31	±	3	180–210	CAM	92.3	±	3.6	4%
MAK/16/14K/2	lakebed	SG	4%	88	67.4	±	2.51	29	±	3	180–210	CAM	85.4	±	10.0	12%
MAK/16/14K/3	lakebed	SG	4%	49	65.1	±	3.47	29	±	5	180–210	CAM	84.9	±	10.5	12%
MAK/16/14K/M1/1	lakebed dune	MG		54	0.10	±	0.01	43	±	5	180–210	MAM3	0.10	±	0.01	14%
MAK/16/14K/M1/2	lakebed dune	MG		33	0.12	±	0.01	126	±	13	180–210	MAM3	0.14	±	0.02	12%
MAK/16/14K/M1/3	lakebed	SG		43	47.6	±	2.59	23	±	6	180–210	CAM	83.5	±	9.6	12%
MAK/16/14K/M2/1	lakebed dune	MG		54	0.08	±	0.01	150	±	15	180–210	MAM	0.10	±	0.01	11%
MAK/16/14K/M2/2	lakebed dune	MG		45	0.10	±	0.01	114	±	12	180–210	MAM	0.12	±	0.01	12%
MAK/16/14K/M2/3	lakebed dune	SG		50	0.19	±	0.02	203	±	24	180–210	FMM	0.17	±	0.03	16%
MAK/16/14K/M2/4	lakebed	SG	3%	47	55.6	±	3.05	31	±	5	180–210	CAM	108.9	±	12.4	11%
MAK/16/14O/1	lakebed	SG	5%	141	59.2	±	1.67	27	±	2	180–210	CAM	105.7	±	3.0	3%
MAK/16/14O/2	lakebed	SG	6%	67	59.3	±	2.68	30	±	4	180–210	CAM	105.3	±	11.1	11%
MAK/16/15/1	lakebed dune	MG		48	0.06	±	0.01	141	±	15	180–210	MAM3	0.08	±	0.01	9%
MAK/16/15/2	lakebed	SG	10%	82	90.1	±	3.78	32	±	3	180–210	CAM	69.9	±	12.1	17%
MAK/16/15/3*	lakebed	SG	38%	40	82.3	±	5.6	38	±	5	180–210	CAM	65.5	±	10.3	16%
MAK/16/6/F1/1	lakebed dune	SG		64	0.46	±	0.03	44	±	6	180–210	CAM	0.33	±	0.02	7%
MAK/16/6/F2/1	lakebed dune	SG		42	0.92	±	0.08	41	±	7	180–210	CAM	0.56	±	0.1	15%
MAK/16/6/F2/2	lakebed dune	SG		70	2.28	±	0.11	29	±	5	180–210	CAM	1.28	±	0.2	14%
MAK/17/2/1	lakebed dune	MG		52	0.15	±	0.01	107	±	11	180–210	MAM	0.15	±	0.01	4%
MAK/17/2/2	lakebed dune	MG		52	0.19	±	0.01	120	±	12	180–210	MAM	0.20	±	0.02	11%
MAK/17/2/3*	lakebed	SG	46%	70	63.0	±	5.0	59	±	6	180–210	CAM	98.9	±	17.3	17%
		MGFG		25	190.6	±	3.7	6	±	2	4–11	CAM	98.15	±	13.53	14%
MAK/17/3/1	lakebed dune	SG		49	0.25	±	0.02	2	±	0.1	180–210	CAM	0.23	±	0.02	9%
MAK/17/3/2	lakebed dune	SG		36	0.27	±	0.04	36	±	16	180–210	CAM	0.27	±	0.05	18%
MAK/17/3/3	lakebed dune	SG		48	0.32	±	0.04	83	±	14	180–210	CAM	0.35	±	0.1	17%
MAK/17/3/4	lakebed	SG	9%	9	117.4	±	15.1	32	±	11	180–210	CAM	102.86	±	18.2	18%
MAK/17/3/5*	lakebed	SG	57%	61	97.2	±	4.8	28	±	5	180–210	CAM	75.0	±	10.5	14%
		MGFG	12%	8	195.1	±	10.3				4–11	CAM	128.0	±	17.7	14%
MAK/17/4/1	lunette	SG		95	2.47	±	0.21	75	±	7	180–210	CAM	2.3	±	0.2	8%
MAK/17/4/2	lunette	SG		147	15.3	±	0.45	30	±	2	180–210	CAM	8.5	±	1.1	13%
MAK/17/4/3	lunette	SG		127	14.3	±	0.71	51	±	4	180–210	CAM	7.8	±	1.1	14%
MAK/17/5/1	ridge	SG		71	2.1	±	0.13	34	±	7	180–210	CAM	2.7	±	0.2	6%
MAK/17/5/2	ridge	SG		49	2.0	±	0.11				180–210	CAM	2.6	±	0.3	11%
MAK/17/5/3	ridge	SG		144	3.9	±	0.21	57	±	5	180–210	FMM	3.8	±	0.5	12%
MAK/17/5/4	ridge	SG		105	11.7	±	0.40	26	±	3	180–210	CAM	11.1	±	1.3	12%
MAK/17/6/1	lakebed dune	SG		60	0.86	±	0.05	7	±	19	180–210	CAM	0.8	±	0.05	5%
MAK/17/6/2	lakebed dune	SG		64	1.31	±	0.06				180–210	CAM	1.1	±	0.1	14%
MAK/17/6/3	lakebed dune	SG		94	1.19	±	0.04	12	±	8	180–210	CAM	1.1	±	0.1	13%
MAK/17/6/4	lakebed dune	SG		64	1.07	±	0.05				180–210	CAM	1.0	±	0.1	14%
MAK/17/6/5	lakebed	SG	5%	101	105.2	±	6.47	189	±	14	180–210	FMM	86.3	±	12.8	15%
MAK/17/7/1	lakebed dune	SG		120	1.98	±	0.11	50	±	5	180–210	CAM	2.0	±	0.1	6%
MAK/17/7/2	lakebed dune	SG		123	1.78	±	0.08	39	±	4	180–210	CAM	2.1	±	0.3	12%
MAK/17/8/1*	lakebed	SG	34%	26	75.6	±	11.3	73	±	11	180–210	CAM	51.9	±	9.3	14%
		MGFG		17	158.4	±	2.5	0	±	0	4–11	CAM	94.2	±	7.2	8%
MAK/17/8/2	lakebed	SG	11%	53	49.6	±	5.7	81	±	8	180–210	CAM	31.1	±	4.4	14%
		MGFG		16	152.8	±	3.0	4	±	3	4–11	CAM	80.5	±	6.1	8%
MAK/17/8/3*	lakebed	SG	58%	39	99.8	±	5.5	26	±	5	180–210	CAM	70.2	±	6.9	10%
		MGFG	5%	21	156.3	±	5.6	15	±	3	4–11	CAM	91.6	±	7.3	8%
MAK/17/9/1*	lakebed	SG	35%	72.0	71.0	±	4.0	40	±	5	180–210	CAM	66.5	±	7.3	11%
		MGFG		5	85.7	±	5.8	13	±	6	4–11	CAM	68.9	±	6.6	8%
MAK/17/9/2*	lakebed	SG	30%	51	69.3	±	3.6	31	±	4	180–210	CAM	72.1	±	7.1	10%
		MGFG		8	83.4	±	2.6	5	±	4	4–11	CAM	72.0	±	5.3	7%
MAK/17/10/1	lakebed	SG	23%	134.0	87.8	±	2.6	17	±	4	180–210	CAM	89.6	±	6.9	8%
		MGFG		13	117.4	±	8.3	22	±	6	4–11	CAM	99.9	±	9.6	10%
MAK/17/11/1*	lakebed	SG	37%	74	86.4	±	6.3	58	±	6	180–210	CAM	64.4	±	7.4	11%
		MGFG	8%	21	135.2	±	5.7	17	±	3	4–11	CAM	86.8	±	7.2	8%
MAK/17/11/2*	lakebed	SG	64%	66	123.4	±	5.3	29	±	4	180–210	CAM	99.1	±	8.9	9%
		MGFG	4%	21	164.5	±	3.8	1	±	27	4–11	CAM	112.5	±	8.3	7%
MAK/17/12/1*	lakebed	SG	41%	76.0	120.6	±	7.3	43	±	5	180–210	CAM	95.3	±	9.6	10%
		MGFG		25	168.5	±	2.4				4–11	CAM	115.3	±	8.5	7%
MAK/17/1a/4	lakebed	MGFG	5%	18	36.2	±	0.8	30	±	7	4–11	CAM	26.8	±	4.2	15%
MAK/17/1a/40	lakebed	MGFG	5%	19	131.2	±	3.8	9	±	3	4–11	CAM	80.6	±	10.3	13%
MAK/17/1a/76	lakebed	MGFG		19	152.7	±	2.8				4–11	CAM	109.5	±	13.06	12%

5. Discussion

5.1. Landscape evolution

5.1.1. Timing of lakebed dune formation

Aeolian deflation of mineral dust (silt) from the Makgadikgadi pans has been well-documented, with the basin known to be the third largest source of dust in the southern hemisphere (Vickery et al., 2013). Richards et al. (2021) used cellular automation modelling in conjunction with OSL dating to show that lakebed dunes accumulate over remnant moist, sticky patches as the pan floor dries out following seasonal rains or flooding. The increased shear velocity threshold associated with wet spots results in the deposition of sand and silt grains blowing across the lake floor as the pan transitions between wet and dry conditions. Once accumulated, the sediments form elevated deposits which increase surface roughness resulting in a positive feedback for sediment deposition (Kocurek and Fielder, 1982). When sediments have built up to a few centimetres above the pan floor, the dune is stabilised by halophytic grasses that encourage further aeolian deposition. This theory combines previous ideas and data (Burrough et al., 2012; Franchi et al., 2020; Grove, 1969; McFarlane and Long, 2015) but suggests, in contrast to these earlier theories, that dune construction occurs at times when the basin floor was drying, and wind-blown sediment was readily available.

The OSL ages from lakebed dunes in this and previous studies suggest these conditions have been met during 2 or 3 distinct periods during the late Holocene but do not preclude this process of dune building from having occurred during low-stands throughout the late Quaternary. For the dunes analysed in this study, sediment first accumulated during the late Holocene at 2.1–2.0 ka and 1.3–0.6 ka (Table 4). This is broadly consistent with previous findings in the Ntwetwe basin where dunes were dated to between 3.4 and 0.8 ka (Burrough et al., 2012; Burrough and Thomas, 2013). A second very recent phase of accumulation has occurred between 350 ± 100 and 30 ± 10 years ago, consistent with dune ages from neighbouring Sua Pan (Richards et al., 2021).

Dune ages at the Ntwetwe Northeast locality seem to increase in a westerly direction, as also noted by Burrough and Thomas (2013) from analyses of dunes on the western side of the Ntwetwe pan. The more elongate dune forms west of the archaeological site MAK33 accumulated parallel to the ridge line (Fig. 3c) between 1.1 ± 0.1 and 0.8 ± 0.1 ka (MAK/17/6). The more linear form of these features is likely caused by increased aeolian sediment supply moving across the basin floor (Richards et al., 2021) and the ridge acting as a topographic barrier to aeolian transport; either scenario would enhance sediment deposition. Neo-tectonism has no doubt affected subsurface groundwater and overland flows that render this part of the basin particularly muddy under present day conditions, contributing to localised 'wet spots'.

5.1.2. Age of the ridge west of site MAK33

OSL ages from the upper sandy sediments of the western margin ridge of the northeastern Ntwetwe spur (at 918 m asl) suggest that 1.5 m of sediment accumulated between 3.8 ± 0.5 and 2.7 ± 0.2 ka. This period of deposition falls within the earlier phase of dune accumulation identified further west by Burrough et al. (2012) and Burrough and Thomas (2013) and is therefore likely due to aeolian processes mobilising sediment from the pan floor and banking it up against the topographic rise to the west. This has created what is effectively a lunette dune. The narrow distribution of the equivalent doses from the upper samples suggests these sediments are undisturbed primary deposits, with a sediment matrix that is unlikely to have been affected by tectonic movement despite their proximity to the horst and graben features to the north of the basin. The sediments overlie older material at 3 m depth dated to 11.1 ± 1.3 ka, which itself is underlain by carbonate-cemented sediments at 3.6 m from the surface. This carbonate surface outcrops in the topographic low between the lunette and the 920 m palaeolake shoreline to the west. All ages for samples from this ridge post-date the MSA suggesting the shoreline and pan margin may have been very different at the time of archaeological deposition on the pan floor at MAK33 and beyond.

5.1.3. Lakebed deposition and preservation

The young ages for the overlying dune landforms stand in stark contrast to the lakebed material near the present-day pan surface, which is much older at both Nwetwe Central and Ntwetwe Northeast.

5.1.3.1. Ntwetwe Northeast. Near surface (<1 m) lakebed sediments in the MAK33 region comprise two to three geochronologically distinct units deposited at 128 ± 18 – 98 ± 14 ka; 94 ± 7 – 81 ± 6 ka and 72 ± 5 – 69 ± 7 ka (all ages within each cluster being indistinguishable within errors, though note there is also some overlap in errors between groups). Sediments dating to 72-69 ka appear to have been patchily preserved (Fig. 8), perhaps protected from deflation by former wet zones and/or overlying lakebed dunes that have since been eroded. Vibracored, shallow lake sediments in a wet zone of the pan 80 m to the northeast of site MAK33 date to 27 ± 4 ka. These younger sediments have been protected from deflation by the wetter surface here.

5.1.3.2. Ntwetwe Central. Within the central Ntwetwe sites, 2–3 lake deposits were identified dating to 109 ± 12 – 105 ± 11 ka; 92 ± 4 ka – 84 ± 10 ka and 70 ± 12 ka – 57 ± 8 ka.

Taking all the OSL ages of the dated lakebed sediments from both Ntwetwe Central and Ntwetwe Northeast, three to four lacustrine periods can be tentatively identified between 128 ± 18 and 27 ± 4 ka. Cluster analyses performed in R using the Partitioning around Medoids method (Kaufman and Rousseeuw, 1990) suggest these periods are centred on c.109 ka (C1, n = 10), 85 ka (C2, n = 11), 66 ka (C3, n = 6) and 27 ka (C4, n = 1). The ages of these deposits bear close affinity to lacustrine phases also documented within palaeolake shoreline records centred on 105 ± 4 ka; 92 ± 2 ka and 64 ± 2 ka (Burrough et al., 2009) and diatom deposits in the Boteti dated to between 103 ± 6 ka and 88 ± 6 ka (Schmidt et al., 2017). While precision on the lake bed ages alone is too poor at this age range to determine if sediments within and between groups relate to a single high lake phase or multiple high lake stands, the presence of in-situ archaeological sites stratigraphically located between cluster C2 and C3 suggest these highstands in particular were distinct (see section 5.2).

5.1.3.3. Deflation and preservation of lacustrine sediment deposits. Dates on near surface lakebed sediments suggest that, in the Ntwetwe Pan, aeolian processes have led to the deflation of lacustrine sediments with strong localised variability. When deflation occurs during lake lowstands, sediment is removed until the water table is reached, or a more resistant sediment layer is exposed (e.g. one cemented by silica or salt). The net deflation in Ntwetwe over the late Quaternary contrasts with Sua Pan where, due to regular inundation, surface sediments have continued to accumulate, the upper sediments dating to the late Holocene (Burrough et al. in prep).

Four of the six ages that document lake deposits between c. 57 and c. 72 ka are from augered samples collected at levels immediately below lakebed dune mounds. The remaining two are associated with a dune 'footprint' on the lakebed floor (see section 1.4.2), suggesting that the sampling area may have been overlain by

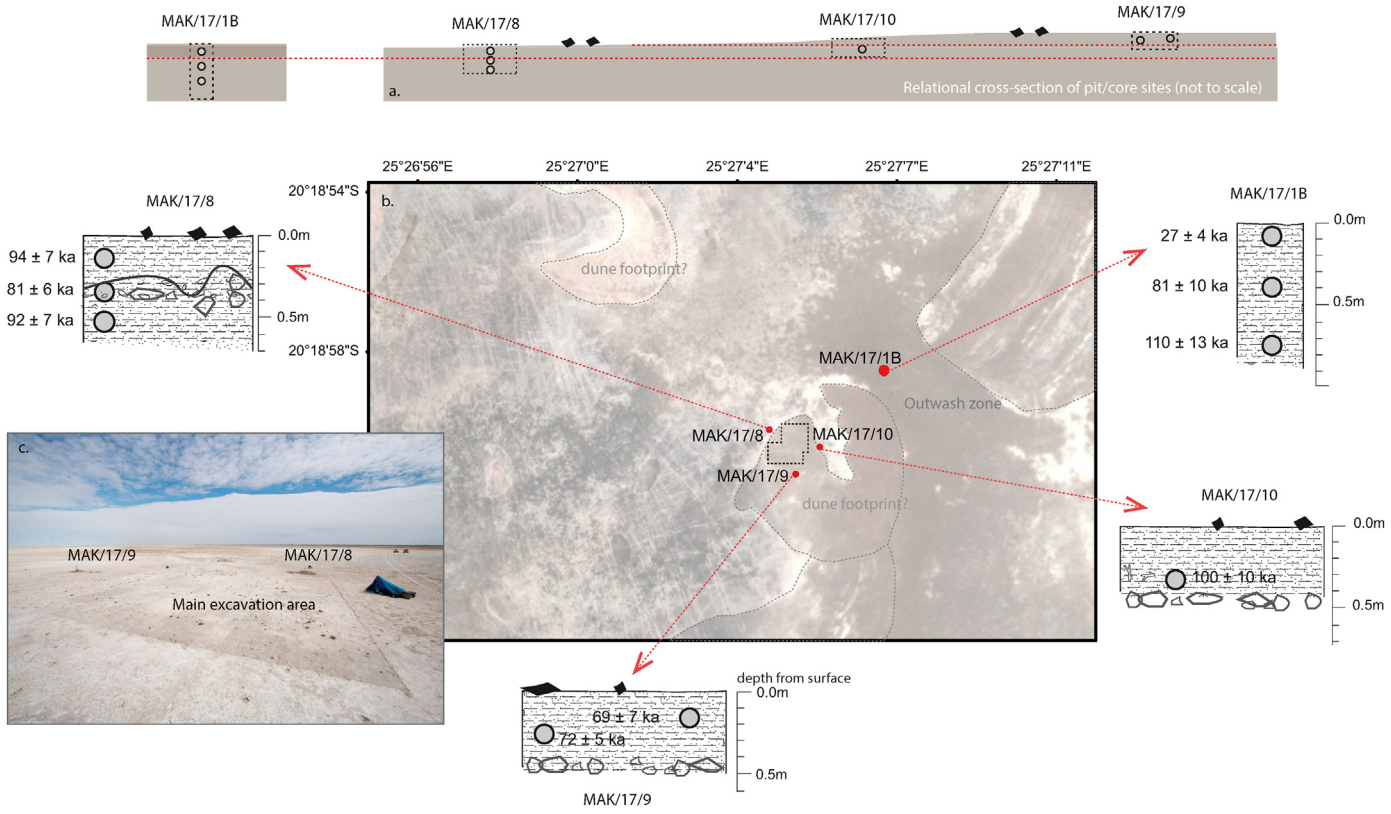

Fig. 8. Archaeological site MAK33 in Ntwetwe Northeast showing a) Schematic of site geomorphology with pit locations also shown as b) map of site locations in relation to zone of main excavation (dotted grey polygon) and chronological/sedimentological data for each site with an inset of image c) looking southwest across the excavation.

a dune landform in the past. That lake sediments immediately beneath dunes are frequently younger than the near surface lake sediments on the exposed pan floor immediately next to them is significant. It leads us to hypothesise that the stabilised dune landforms have protected surface lacustrine sediment from deflation during the last 350 years (the maximum age of these dune deposits). Where lacustrine sediment has not been overlain by a dune, deflation has exposed MSA sites on the lakebed. Where this exposure has occurred recently, such as at the sites investigated in this study, the MSA material appears fresh and relatively undisturbed. Artefacts at these sites certainly lack the intensive geochemical weathering that would be expected to affect silcrete had it been exposed at the surface for 60–70 kyrs, as would be suggested by the quiescent model of lake evolution (see section 2.2).

5.2. Timing of human use of the lakebed

In the majority of archaeological sites reported here, dated lake sediments lie below the Stone Age archaeological material, allowing only maximum ages to be placed on the archaeology and the use of the lake floor by Stone Age humans (see Table 5).

5.2.1. Ntwetwe Northeast

Analysis of the lithic assemblage at MAK33 suggests limited post-depositional disturbance, which indicates the material has not seen extensive spatial movement through post-depositional processes (Staurset et al., 2022b). The artefact assemblage also shows no within-site variability that would suggest multiple site visits. As part of this assemblage overlies the younger lake sediments dated to 72-69 ka (Fig. 8), we therefore infer that the MSA archaeology at MAK33 post-dates this lake phase, with subsequent progressive deflation of the lacustrine material over some of the site causing a few cm of 'lowering' of the archaeology on to a more resistant lacustrine unit.

5.2.2. Ntwetwe Central

Makgadikgadi archaeological sites are characteristically open. Placing a minimum age on both the MSA use of the basin floor and the lake lowstand during which it occurred is challenging unless we are able to find buried archaeological material in-situ. Site MAK14K, has, however, enabled us to make some inference about the limits of human use of the basin during a low stand. An investigative trench dug into the lakebed dune adjacent to this site revealed a silcrete flake fragment located between two chronostratigraphically distinct lakebed deposits. This artefact lay on top of muddy lakebed sands deposited at 84 ± 10 ka that extended out into the main site where these sediments were also dated to between 85 ± 10 and 92 ± 4 ka. The artefact was then buried during a subsequent lake highstand that deposited silty sands over the site, some of which are still present and dating to between 57 and 59 ± 8 ka. These latter sediments are not preserved within the adjacent open-air context (Fig. 9) due to deflation, as discussed in section 4.3. At this site, it is therefore possible to place the window of occupation within an ~25 kyr period between 84 ± 10 and 59 ± 8 ka. This is important, not least because palaeolake records in arid or semi-arid areas often only record periods of high lake-stands and offer little preserved evidence of dry periods when lake levels were low or basins were empty (De Cort et al., 2021).

At a separate site (MAK15), a single artefact was found on the surface of lake sediments that dated to between 70 ± 12 ka and 66 ± 10 but was underlying an 80-year-old dune. The most

Table 5
Ages of sediments associated with investigated archaeological sites, constraining the age of the archaeological material. The figure in brackets refers to the cluster of lake ages representing lake high stands (Fig. 10) to which the date belongs.

Archaeological Site ID	Archaeological Context	Minimum Archaeological Age/Age of overlying sediments (ka)	Maximum Archaeological Age/Age of underlying sediments (ka)
MAK15	MSA		70 ± 12 (C3)
MAK14K	MSA	59 ± 8	84 ± 10 (C4)
MAK14O	MSA		106 ± 3 (C4)
MAK33	MSA		69 ± 7 (C3)
MAK6	LSA	0.33 ± 0.02	1.28 ± 0.2

parsimonious explanation for this is that artefacts at this site were deposited sometime after the lake phase that buried the archaeological material at MAK14K.

Overall, site analyses in this study tentatively suggest that MSA archaeological sites in the pan both post-date (overlie) and pre-date (underlie) lake sediments deposited during a lake high-stand that occurred sometime between c.57 and c.72 ka (C3). This high-stand is documented within shoreline records, that infer lake levels between 60 ± 6 and 66 ± 5 ka were 37–39 m above the present lake floor (Burrough et al., 2009; De Cort et al., 2021) (Fig. 10). Therefore, while each site represents only a single visit, MSA people may have repeatedly used the basin during periods where lake levels were very low. We note that, in the future, more sites where bracketing ages can be established on archaeological material would enable the timing of site occupations to be established with greater precision and robustness.

The late Holocene ages (2.1–2.0 ka, 1.3–0.6 ka and 350-30 years ago) of the sand dunes associated with Makgadikgadi archaeological sites suggests these landforms were not directly responsible for preserving the archaeological material. Instead, we suggest that the lacustrine sediment deposited during lake high stands covered archaeological sites soon after material was left on the basin floor. The later lake sediments have, subsequently protected artefacts for tens of thousands of years. In the last few centuries, dry conditions and a strongly negative water balance (De Cort et al., 2021) have resulted in the deflation of these silty sands from the lakebed, exposing the previously buried archaeological sites, in their relatively undisturbed state. At locations where the lake deposits were then overlain by late Holocene dunes, the lake surface sediments were protected from deflation and patches of the younger, 57–72 ka, lakebed material remain preserved. At other locations, not excavated in this study, exposure of artefacts may have occurred much earlier, and archaeological material will be more heavily disturbed and weathered. Deflationary contexts within open air sites such as this are generally poorly investigated within southern Africa though archaeological information can be very rich when significant effort is placed on understanding post-depositional processes, as at the site of Geelbek in South Africa (Fuchs et al., 2008).

The ages for MSA material in the Makgadikgadi are broadly consistent both with mitogenomic evidence, which suggests a stable population of humans in the region after 110 ka (Chan et al., 2019), and with previously reported ages from four dated sites within the Middle Kalahari basin (White Paintings Cave, Tsodilo, ≠Gi, Toteng and Chavuma – see Fig. 10) yielding MSA archaeology). These span the period between 94 ± 9 ka at White Paintings Shelter in the Tsodilo Hills (L H Robbins et al., 2000) and 52 ± 7 ka at Toteng near Lake Ngami (Brook et al., 2008) (Fig. 10).

5.3. *Influence of landform processes on the potential preservation and visibility of archaeological material within and around the basin*

The OSL ages presented here, together with the analysis of the archaeological material (Staurset et al., 2022a), are strong evidence for human use of the palaeolake basin during times of relatively dry conditions. These were perhaps similar to the seasonally dry conditions that characterise the basin today, when there is the potential for shallow standing water bodies (<908 m asl) as part of the present-day hydrological system. This arises as a residual of wet-season floods, out of season rains, and/or a slowly travelling flood wave that delivers surface flow via the Okavango Delta and Boteti river from the Angolan Highlands, peaking in the winter dry season (Pekel et al., 2016; see section 2.1). This pattern of surface water distribution may have been similar for dry periods in the late Pleistocene and would have provided an important resource for animal populations in the Middle Kalahari. Historically, animals have moved from dry season permanent water bodies to temporary water holes in the wet season grasslands; this included millions of springbok and wildebeest that moved hundreds of km from the central to the southwest Kalahari and hundreds of thousands of zebra and wildebeest that seasonally migrated from the Boteti River to wet season pools in the Makgadikgadi grasslands (Bartlam-Brooks et al., 2011). These wetlands within a dry environment no doubt offered an important resource to human populations during periods when the palaeolake was absent.

Brooks (1984) investigated the varying seasonal landscape use by modern Juc'hoansi (!Kung) San in the northwest Kalahari and found that groups that were dispersed and highly mobile during the wet season aggregated near water during the dry season. These aggregation camps, at resource-rich sites, are occupied for longer periods of time, leaving a more visible record of usage than wet season sites. The implication is that, if these patterns hold for prehistory, archaeological visibility in the landscape should strongly correlate with areas where water is available during Late Pleistocene dry phases (Burrough, 2016) because of repeated or prolonged occupation. However, analysis of the archaeological material suggests individual sites within the Makgadikgadi were not repeatedly used, or indeed used for long periods of time. Our understanding of landform evolution from this study suggests instead that the distribution of archaeological sites in the present-day landscape is determined not only by the distribution of food/water resources at the time of deposition but is also strongly affected by the presence or absence of depositional landforms and post depositional processes that have occurred since site formation. These processes have effectively amplified the visibility of archaeological material along river courses and within lakebeds/pans but tended to bury and subdue archaeological signals outside of these areas, such as on the shore zones and lake ridges or areas containing a large number of dunes.

While the Ntwetwe Pan floor has periodically, during high lake stands, been a zone of deposition, the cumulative processes

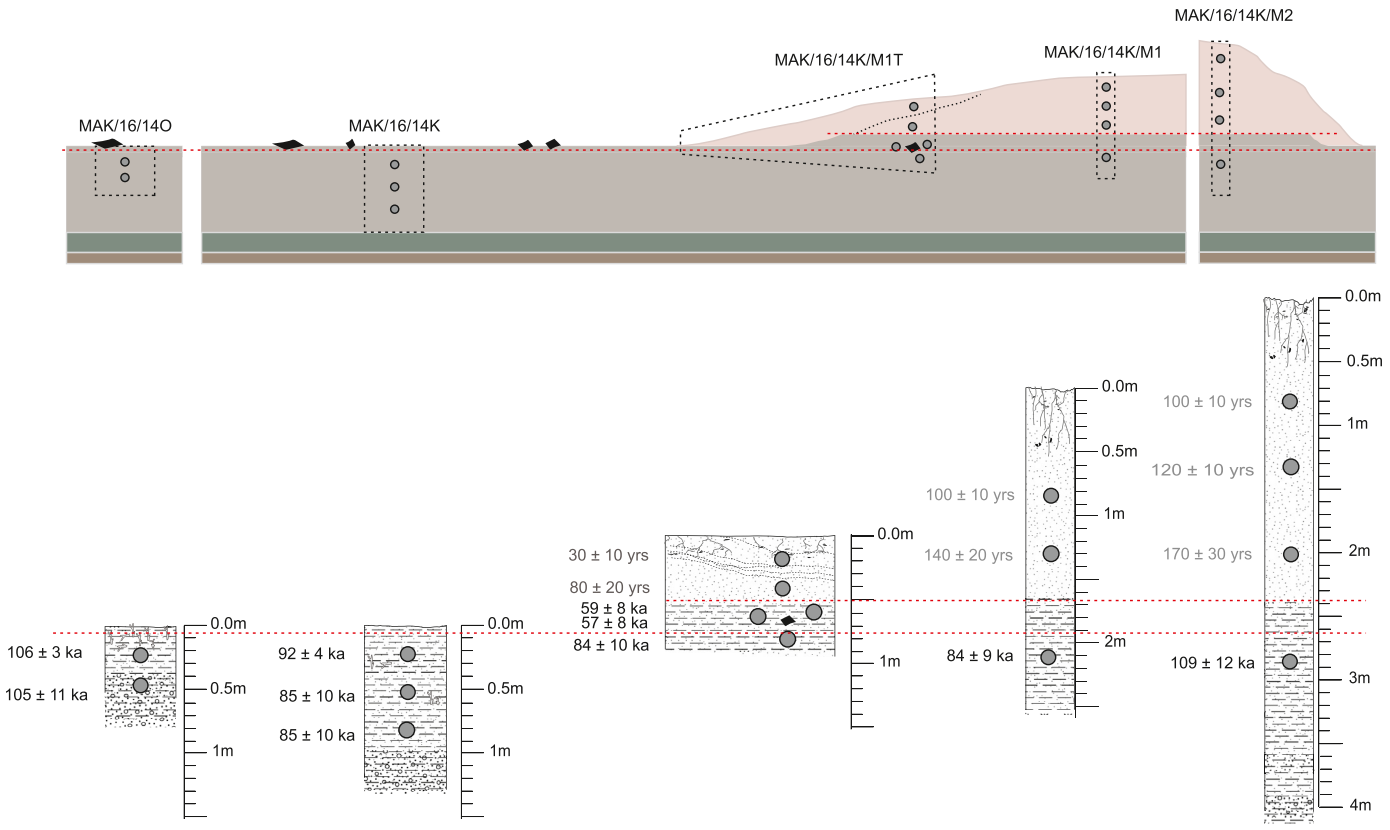

Fig. 9. Sections and OSL ages at archaeological site MAK14K and MAK14O in Ntwetwe Central.

operating here over the last 60,000 years have resulted in net deflation, exposing sediments and sites laid down in the Middle Stone Age. In contrast, the vegetated shore zone and landforms overlying the surface of the pan (e.g. the lunette ridge northwest of MAK33) represent areas of net accumulation. We do not find MSA sites on the surface here because these sediments appear to have mostly accumulated in the last 11,000 years. The underlying sediments within these areas may harbour MSA material, but they are not visible to us using standard archaeological surveys. This pattern of visibility is also true for fluvial systems (e.g. Burrough et al., 2019) – including those leading directly into the basin – where surface flows result in net erosion close to the channel, as opposed to the net deposition in areas further from channelised flow.

Within the pan floor itself, the process of deflation is patchy and variable at the small (metre by metre) scale. However, a growing bank of geochronological data in conjunction with present-day observations suggests that some regions of the Makgadikgadi pan floor are more likely to be zones of net-deflation while others are zones of net-accumulation. Recent research in Sua Pan (Burrough et al. in prep) suggests several metres of sediments have accumulated and survived deflation since the Last Glacial Maximum. Like Sua Pan, the southern and eastern side of Ntwetwe Pan is frequently inundated with standing water, which both protects surface sediments from deflation and brings fresh sediments into the system. It is in these zones of the pan floor that MSA material is less visible both because i) a similar pattern of surface water may have prevailed in the past and ii) MSA sites that do exist are likely buried beneath several metres of sediment.

The consequence of this is that archaeological data will be predisposed to recording activities that occurred during dry times on the lake floor rather than on the shorelines during lake high-stands. At the basin margins in the west and the north, the oldest ages for the upper 1 m of sediments on the highest lake level palaeoshorelines also post-date the MSA, at c. 39 ka, 28 ka, 19 ka and 8 ka (Burrough et al., 2009). The use of the landscape during periods where lake levels were high may have been very different. Encouragingly, however, this study suggests that if we are able to find MSA shoreline sites, their in-situ burial would allow us to establish a much more precise chronological record of site formation, though their preservation potential is dependent on how quickly and completely such sites were buried. If present, it should only be possible to find MSA sites buried within the basin shorelines, perhaps, for example, during the lake high-stands that are recorded in the shorelines between 66 ± 5 ka and 62 ± 8 ka and 105 ± 4 ka and 92 ± 2 ka. On the innermost Gidikwe ridge, at the western margin of the Makgadikgadi, sediments of these ages occur between 3.5 and 4 m and 4.5–6 m depth respectively from the vegetated ridge surface. Future excavations will be informed by our improved understanding of the spatial dynamics of sediment deposition, deflation and erosion, maximising the potential for discovery of in-situ material that provides a window into how humans used the landscape during both wet high-lake periods as well as during dry, low-lake conditions in the basin.

5.4. Dynamic vs quiescent late quaternary lake system

One of the most important findings from this study is that archaeological material was buried and preserved by sediments deposited during lake high-stands and then re-exposed, in many cases, very recently, by deflation during dry times. The relatively undisturbed archaeological sites investigated here are found in this state because of their specific post-depositional context. They have been buried by lake sediments for the majority of time since their formation. Where archaeological material on the pan floor is

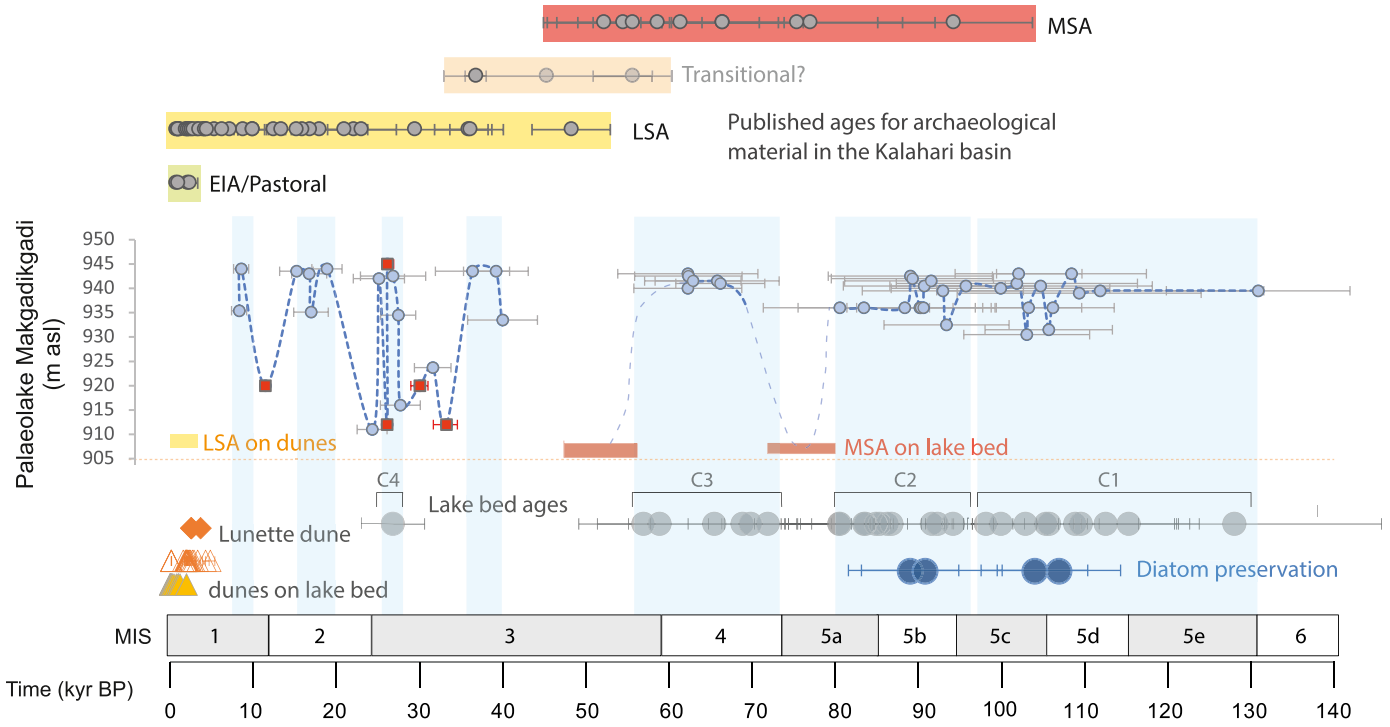

Fig. 10. *Age of lakebed and MSA archaeology in relation to existing records of lake level change, and Stone Age Archaeology reported in the Kalahari basin* (Brooks et al., 1990; Burrough et al., 2019; Feathers, 1997, 2015; Ivester et al., 2010; Lukich et al., 2019; Robbins et al., 1996, 2000, 2008; L.H. Robbins et al., 2000; Robbins and Campbell, 1989; Yellen and Brooks, 1989). *Where ^{14}C ages were reported in the literature, the ages were recalibrated using age-depth models for sediment profiles in conjunction with the SH20 calibration curve and Bayesian age-depth modelling software Bacon in R* (Blaauw and Christeny, 2011; R-Development-Core-Team, 2020). *Note that due to sediment mixing, the 'transitional' nature of archaeological deposits at Tsodilo has been questioned at White Paintings Rock Shelter* (Staurset and Coulson, 2014). *The lake level curve for the Makgadikgadi (dashed blue line) does not include the interconnected Ngami and Mababe sub-basins. It is reconstructed from OSL ages on shorelines (blue dots, uncertainties shown as grey error bars) and re-calibrated radiocarbon ages (red squares, uncertainties shown as red error bars)* (Burrough et al., 2009; Cooke and Verstappen, 1984; Ringrose et al., 2005; Shaw et al., 1992) *The chronology of diatom deposits* (Schmidt et al., 2017), *and landform ages within the basin (this study) are shown below the lake level curve (grey circles = lakebed ages and their associated clusters (C1-4); orange diamonds = lunette dune ages; filled yellow triangles = dune ages (this study); open orange triangles = dune ages from Burrough and Thomas, 2013).* (For interpretation of the references to colour in this figure legend, the reader is referred to the Web version of this article.)

disturbed and weathered, it has likely been exhumed and exposed to both mechanical and geochemical processes for a greater proportion of the time since burial. This discovery does not allow us, from this study alone, to infer either the magnitude or the frequency of fluctuating lake levels since the MSA sites were formed. It does, however, suggest we should reject the inference that MSA archaeological sites on the bed of Makgadikgadi are evidence alone for a lack of lake level fluctuations (the *Quiescent model* described in section 1.2) in the time since MSA humans occupied this landscape.

5.5. Primary controls on climate/environmental variability in the interior

Chan et al. (2019) suggested from model data and ocean cores averaged over the entire southern African continent that the regional divergence of climatic and environmental conditions was the primary driver of population movement out of the interior, as observed in their mitogenomic timelines. Specifically, they infer from ocean core records and climate model data that the Makgadikgadi region became dry during the period between 110 and 80 ka, creating conditions of reduced carrying capacity for MSA humans. Lake level data from Makgadikgadi does not support this conclusion, with high lake stands evident from dated shorelines (n = 14) (Burrough et al., 2009) and ages from lakebed lacustrine sediments (this study, n = 20) occurring between 115 ± 8 ka and 81 ± 6 ka Fig. 10. Our data suggests the basin dried out a little later than this, at some point between 81 ± 6 ka and 72 ± 5 ka and that MSA humans in the region were using the lakebed during this time. The lake again dried out sometime after 57 ± 8 ka and again MSA humans used the lakebed sometime after this. Makgadikgadi, however, is part of a complex hydrological system with a catchment that spans a huge region of the southern African interior. Simply invoking local climate change alone as a push or pull factor on human populations at this time is oversimplistic: Palaeolake transgressions and regressions may well be out of phase with localised climate shifts (Burrough et al., 2009), a characteristic of the basin that remains poorly understood.

6. Conclusions

MSA humans used the Makgadikgadi basin during dry times when lake levels were very low or seasonal. At one site (MAK14K) this period of occupation is identified as having occurred within the window of time between 84 ± 10 ka and 59 ± 8 ka, between two lake high stands centred on c.85 ka and 66 ka. At two other sites, MAK15 and MAK33, occupation occurred sometime after the lake high stand centred on c.66 ka. Determining OSL ages of landforms in the Makgadikgadi associated with archaeological sites is challenging as sediments lie at both the upper and lower limits of quartz OSL dating. A paucity of feldspar and a high degree of residual dose rendered post IR-IRSL feldspar dating similarly exigent, though larger sample sizes may help to negate some of these drawbacks in future. Despite age uncertainties, the pattern and timing of landform emplacement suggests dunes and lunettes on the present-day pan margin post-date archaeological sites, such that geomorphological configuration of the basin at the time of

MSA occupation would have been very different. This simultaneously explains the absence of MSA artefacts on the surface of those landforms. Landform OSL ages also suggest that archaeological sites are rapidly buried by lake deposits during subsequent high lake stands and exposed during dry periods where deflation is dominant. Where exposure has occurred very recently, sites are relatively undisturbed and archaeological material appears fresh.

This cyclical burial and exposure allows us to reject the presence of archaeology in the basin as evidence for a wholly quiescent dry lakebed during the late Quaternary. While quantifying either the frequency or magnitude of lacustrine periods during this period remains challenging, the weight of evidence (including shoreline OSL ages, diatom deposits and ages on lakebed sediments) still favours a dynamic lacustrine system that responded to large-scale climate shifts and/or tectonic events. Future lake-drilling efforts may help to resolve the structure of such large-scale hydrological changes within the last 200 kyrs.

The resource limits of this research have not allowed extensive survey or excavation of known palaeo-shorelines. Bias in site visibility due to patterns of net sediment accumulation (e.g. at the shorelines or in Sua Pan) vs areas of net-deflation (e.g. Ntwetwe Pan floor) where archaeological sites are readily exposed, has meant we are not yet able to comparatively examine how people used the Makgadikgadi basin during wet (high-lake) periods.

Recent controversial research (Chan et al., 2019) uses model data to infer that for 70 kyrs the Makgadikgadi sustained the deepest-branching maternal founder populations of Anatomically Modern Humans, with increased humid periods to the northeast and southwest allowing successful out-migrations between 130 and 110 ka. The authors then proposed that the Makgadikgadi experienced subsequent drying from 110 to 80 ka that further pushed populations to move out of the area, though a sustained constant effective population remained. The OSL ages associated with archaeological sites in this study support the notion that humans remained present in the region even when dry conditions prevailed. However, dates on lacustrine deposits suggest local hydrological conditions did not act as a push factor and that high lake levels prevailed between 110 and 80 ka (in contrast to the dry environment suggested by Chan et al., 2019).

While there are still many questions left unanswered, the systematic approach taken in this study has enabled us to reject the idea that there is little to learn from open air sites in the dryland interior. Dry lakebeds offer an important window into these poorly investigated regions and a relatively accessible environment in which to redress the bias in archaeological research in southern Africa that has long focused on the continental margins.

Author contributions

Sallie Burrough: Conceptualization, Investigation, Formal analysis, Writing – original draft preparation, Supervision. David Thomas: Writing – review & editing, Project administration, Conceptulization, Supervision. Josh Allin: Investigation, Formal Analysis. Sheila Coulson: Writing – review & editing; Sarah Mothulatshipi: Supervision, Investigation, Resources, Writing - review & Editing; David Nash: Writing – review & editing; Sigrid Staurset: Writing – review & editing.

Declaration of competing interest

The authors declare that they have no known competing financial interests or personal relationships that could have appeared to influence the work reported in this paper.

Acknowledgements

Fieldwork was carried out under research permit EWT 8/36/4 XXXV (9), issued April 22, 2016 by the Botswana Ministry of Environment, Wildlife and Tourism (ref EWT 8/36/4 XXXV (52)), extended on June 29, 2018 by the Botswana Ministry of Environment, Natural Resources, Conservation and Tourism (ref ENT 8/36/4 XXXXII (43)).

The project was funded by Research Project Grant RPG-2015-344 awarded by the Leverhulme Trust. Additional funding and resources were gratefully received from the University of Botswana, the University of Oxford, the University of Brighton, and the University of Oslo. The archaeological aspects of the project would not have been possible without the significant contribution to fieldwork by students from the University Botswana including Topo Mpho Chengeta, Cathy Legabe, Casper Lekgetho, Jane Masisi, Agang Motlaleng and Oratile Rt Ramore.

SLB would also like to acknowledge contributions from the Returning Carers Fund and the Trapnell Fund, at the University of Oxford. We also wish to acknowledge the support of the National Museum of Botswana for laboratory space and equipment loans. Our appreciation goes to the local communities of Gweta and Nata and to Ralph Bousfield and Natural Selection for generous advice, access to the field research station, facilities and storage, and field assistance. We also thank the owners and staff of Gweta Lodge for field assistance and sharing of local knowledge and assistance with community engagement. Finally we would like to thank two anonymous reviewers for their positive and helpful suggestions to improve the manuscript.

Appendix A. Supplementary data

Supplementary data to this article can be found online at https://doi.org/10.1016/j.quascirev.2022.107662.

References

Aitken, M.J., 1985. Thermoluminescence Dating. Academic Press, London and New York.

Armitage, S.J., Bristow, C.S., Drake, N.A., 2015. West African monsoon dynamics inferred from abrupt fluctuations of Lake Mega-Chad. Proc. Natl. Acad. Sci. U.S.A. 112, 8543–8548. https://doi.org/10.1073/pnas.1417655112.

Arnold, L.J., Roberts, R.G., Galbraith, R.F., DeLong, S.B., 2009. A revised burial dose estimation procedure for optical dating of youngand modern-age sediments. Quat. Geochronol. 4, 306–325. https://doi.org/10.1016/j.quageo.2009.02.017.

Bartlam-Brooks, H.L.A., Bonyongo, M.C., Harris, S., 2011. Will reconnecting ecosystems allow long-distance mammal migrations to resume? A case study of a zebra Equus burchelli migration in Botswana. Oryx 45, 210–216. https://doi.org/10.1017/S0030605310000414.

Berger, G.W., 1990. Effectiveness of natural zeroing of the thermoluminescence in sediments. J. Geophys. Res. 95 (12), 312–375, 397.

Blaauw, M., Christeny, J.A., 2011. Flexible paleoclimate age-depth models using an autoregressive gamma process. Bayesian Anal 6, 457–474.

Bond, G., Summers, R., 1954. A late stillbay hunting camp on the Nata River, bechuanaland protectorate. South african archaeol. Bull. (Arch. Am. Art) 9, 89–95.

Bradley, J.T., 2012. The Effect of Environmental Variability on the Foraging Behaviour of Plains Zebra (Equus Quagga) in the Makgadikgadi. Botswana. PQDT - UK Irel.

Brook, G.A., Srivastava, P., Brook, F.Z., Robbins, L.H., Campbell, A.C., Murphy, M.L., 2008. OSL chronology for sediments and MSA artefacts at the Toteng quarry, Kalahari Desert, Botswana. S. Afr. Archaeol. Bull. 63, 151–158.

Brooks, A.S., 1984. San land-use patterns, past and present: implications for southern African prehistory. In: Hall, M., Avery, G., Avery, D.M., Wilson, M.L., Humphreys, G.S. (Eds.), Frontiers: Southern African Archaeology Today, vol. 207. BAR International Series, pp. 40–52.

Brooks, A.S., Hare, P.E., Kokis, J.E., Miller, G.H., Ernst, R.D., Wendorf, F., 1990. Dating Pleistocene Archeological Sites by Protein Diagenesis in Ostrich Eggshell, vol. 248, pp. 60–64.

Burrough, S.L., 2016. Late Quaternary environmental change and human occupation of the southern African interior. In: Jones, S., Stewart, B.A. (Eds.), Africa from MIS 6-2: Population Dynamics and Paleoenvironments. Springer, Dordrecht, pp. 161–174.

Burrough, Sallie, L, 2022. The Makgadikgadi Basin. In: Eckardt D, F (Ed.), Landscapes and Landforms of Botswana. Springer, Switzerland, pp. 77–90.
Burrough, S.L., Thomas, D.S.G., 2008. Late quaternary lake-level fluctuations in the Mababe depression: middle kalahari palaeolakes and the role of Zambezi inflows. Quat. Res. 69, 388–403.
Burrough, S.L., Thomas, D.S.G., 2013. Central southern Africa at the time of the African Humid Period: a new analysis of Holocene palaeoenvironmental and palaeoclimate data. Quat. Sci. Rev. 80, 29–46. https://doi.org/10.1016/j.quascirev.2013.08.001.
Burrough, S.L., Thomas, D.S.G., Bailey, R.M., 2009. Mega-lake in the kalahari: a late Pleistocene record of the palaeolake Makgadikgadi system. Quat. Sci. Rev. 28, 1392–1411. https://doi.org/10.1016/j.quascirev.2009.02.007.
Burrough, S.L., Thomas, D.S.G., Bailey, R.M., Davies, L., 2012. From landform to process: morphology and formation of lake-bed barchan dunes, Makgadikgadi, Botswana. Geomorphology 161–162, 1–14.
Burrough, S.L., Thomas, D.S.G., Barham, L.S., 2019. Implications of a new chronology for the interpretation of the middle and later stone age of the upper Zambezi valley. J. Archaeol. Sci. Reports 23, 376–389. https://doi.org/10.1016/j.jasrep.2018.10.016.
Buylaert, J.P., Jain, M., Murray, A.S., Thomsen, K.J., Thiel, C., Sohbati, R., 2012. A robust feldspar luminescence dating method for Middle and Late Pleistocene sediments. Boreas 41, 435–451. https://doi.org/10.1111/j.1502-3885.2012.00248.x.
Chan, E.K.F., Timmermann, A., Baldi, B.F., Moore, A.E., Lyons, R.J., Lee, S.S., Kalsbeek, A.M.F., Petersen, D.C., Rautenbach, H., Förtsch, H.E.A., Bornman, M.S.R., Hayes, V.M., 2019. Human origins in a southern African palaeo-wetland and first migrations. Nature 575 (7781), 185–189. https://doi.org/10.1038/s41586-019-1714-1.
Chase, B.M., Faith, J.T., Mackay, A., Chevalier, M., Carr, A.S., Boom, A., Lim, S., Reimer, P.J., 2018. Climatic controls on later stone age human adaptation in africa's southern Cape. J. Hum. Evol. 114, 35–44. https://doi.org/10.1016/j.jhevol.2017.09.006.
Chazan, M., Wilkins, J., Morris, D., Berna, F., 2012. Bestwood 1: a newly discovered earlier stone age living surface near kathu, northern Cape province, South Africa. Antiquity 86.
Cooke, H.J., Verstappen, T.H., 1984. The landforms of the western Makgadikgadi basin in northern Botswana, with a consideration of the chronology of the evolution of Lake Palaeo-Makgadikgadi. Zeitschrift fur Geomorphol 28, 1–19.
Cotterill, F.P.D., De Wit, M.J., 2011. Geoecodynamics and the kalahari epeirogeny: linking its genomic record, tree of life and palimpsest into a unified narrative of landscape evolution. S. Afr. J. Geol. 114, 489–514. https://doi.org/10.2113/gssajg.114.3-4.489.
Coulson, S.D., Staurset, S., Mothulatshipi, S., Burrough, S.L., Nash, D.J., Thomas, D.S.G., 2022. Thriving in the Thirstland: new stone age sites from the middle kalahari, Botswana. Quaternary Science Reviews Special Issue (under review).
De Cort, G., Chevalier, M., Burrough, S.L., Chen, C.Y., Harrison, S.P., 2021. An uncertainty-focused database approach to extract spatiotemporal trends from qualitative and discontinuous lake-status histories. Quat. Sci. Rev. 258. https://doi.org/10.1016/j.quascirev.2021.106870.
Drake, N.A., Lem, R.E., Armitage, S.J., Breeze, P., Francke, J., El-Hawat, A.S., Salem, M.J., Hounslow, M.W., White, K., 2018. Reconstructing palaeoclimate and hydrological fluctuations in the Fezzan Basin (southern Libya) since 130 ka: a catchment-based approach. Quat. Sci. Rev. 200, 376–394. https://doi.org/10.1016/j.quascirev.2018.09.042.
Du Toit, A.L., 1933. Crustal movements as a factor in the evolution of South Africa. S. Afr. J. Sci. 24, 88–101.
Duller, G, 2003. Distinguishing quartz and feldspar in single grain luminescence measurements. Radiat. Meas. 37 (2), 161–165.
Ebert, J.I., 1979. The significance of archaeological sites located near or in association with ancient strandlines of lake Makgadikgadi, Botswana. Nyame Akuma 15, 2–9.
Ebert, J.I., Hitchcock, R.K., 1978. Ancient lake Makgadikgadi, Botswana: mapping, measurement and palaeoclimatic significance. Palaeoecol. Afr. 10–11, 47–56.
Eckardt, F.D., Cotterill, F.P.D., Flügel, T.J., Kahle, B., McFarlane, M., Rowe, C., 2016. Mapping the surface geomorphology of the Makgadikgadi rift zone (MRZ). Quat. Int. 404, 115–120. https://doi.org/10.1016/j.quaint.2015.09.002.
Ecker, M., Bank, C.-G., Chazan, M., Chen, Y., Green, C., Morris, D., Stoikopoulos, N., Shadrach, K., Stratford, D., Duke, H., 2021. Revisiting pniel 6: the 2017–2019 excavations. South african archaeol. Bull. (Arch. Am. Art) 76, 57–69.
Feathers, J., 2015. Luminescence dating at Diepkloof Rock Shelter - new dates from single-grain quartz. J. Archaeol. Sci. 63, 164–174. https://doi.org/10.1016/j.jas.2015.02.012.
Feathers, J.K., 1997. Luminescence dating of sediment samples from white Paintings rockshelter, Botswana. Quat. Sci. Rev. 16, 321–331.
Folk, R.L., Ward, W.C., 1957. Brazos River bar: a study in the significance of grain size parameters. J. Sediment. Petrol. 27, 3–26.
Franchi, F., MacKay, R., Selepeng, A.T., Barbieri, R., 2020. Layered mound, inverted channels and polygonal fractures from the Makgadikgadi pan (Botswana): possible analogues for Martian aqueous morphologies. Planet. Space Sci. 192. https://doi.org/10.1016/j.pss.2020.105048.
Fuchs, M., Kandel, A.W., Conard, N.J., Walker, S.J., Felix-Henningsen, P., 2008. Geoarchaeological and chronostratigraphical investigations of open-air sites in the Geelbek Dunes, South Africa. Geoarchaeology 23, 425–449. https://doi.org/10.1002/gea.20226.
Grove, A.T., 1969. Landforms and climate change in the kalahari and ngamiland. Geogr. J. 135, 191–212.
Guérin, G., Mercier, N., Adamiec, G., 2011. Dose-rate conversion factors: update. Anc. TL 29, 5–8.
Guérin, G., Mercier, N., Nathan, R., Adamiec, G., Lefrais, Y., 2012. On the use of the infinite matrix assumption and associated concepts: a critical review. Radiat. Meas. 47, 778–785. https://doi.org/10.1016/j.radmeas.2012.04.004.
Guo, Y.J., Li, B., Zhang, J.F., Yuan, B.Y., Xie, F., Roberts, R.G., 2017. New ages for the upper palaeolithic site of Xibaimaying in the nihewan basin, northern China: implications for small-tool and microblade industries in north-east asia during marine isotope Stages 2 and 3. J. Quat. Sci. 32, 540–552. https://doi.org/10.1002/jqs.2949.
Helgren, D.M., Brooks, A.S., 1983. Geoarchaeology at Gi, a middle stone age and later stone age site in the Northwest Kalahari. J. Archaeol. Sci. 10, 181–197. https://doi.org/10.1016/0305-4403(83)90051-1.
Hitchcock, R.K., 1982. The Ethnoarchaeology of Sedentism: Mobility Strategies and Site Structure Among Foraging and Food Producing Populations in the Eastern Kalahari Desert, Botswana. ProQuest Diss. Theses. The University of New Mexico, Ann Arbor.
Hitchcock, R.K., Crowell, A.L., Brooks, A.S., Yellen, J.E., Ebert, J.I., Osborn, A.J., 2019. The ethnoarchaeology of ambush hunting: a case study of ǂGi Pan, western ngamiland, Botswana. Afr. Archaeol. Rev. 36, 119–144. https://doi.org/10.1007/s10437-018-9319-x.
Ivester, A.H., Brook, G.A., Robbins, L.H., Campbell, A.C., Murphy, M.L., Marais, E., 2010. A sedimentary record of environmental change at Tsodilo Hills white Paintings rock shelter, northwest Kalahari desert, Botswana. Palaeoecol. Afr. 30, 53–78.
Jacobs, Z, Roberts, R, 2009. Catalysts for Stone Age innovations: What might have triggered two short-lived bursts of technological and behavioral innovation in southern Africa during the Middle Stone Age? Communicative and Integrative Biology 2 (2), 191–193.
Kaufman, L., Rousseeuw, P.J., 1990. Partitioning around Medoids (program PAM). In: Kaufman, L., Rousseeuw, P.J. (Eds.), Finding Groups in Data: an Introduction to Cluster Analysis. John Wiley & Sons, Hoboken, USA, pp. 68–125.
Kocurek, G., Fielder, G., 1982. Adhesion structures. J. Sediment. Petrol. 52, 1229–1241.
Lukich, V., Cowling, S., Chazan, M., 2020. Palaeoenvironmental reconstruction of Kathu Pan, South Africa, based on sedimentological data. Quat. Sci. Rev. 230, 106153. https://doi.org/10.1016/j.quascirev.2019.106153.
Lukich, V., Porat, N., Faershtein, G., Cowling, S., Chazan, M., 2019. New chronology and stratigraphy for kathu Pan 6, South Africa. J. Paleolit. Archaeol. 2, 235–257. https://doi.org/10.1007/s41982-019-00031-7.
Marean, C.W., Cowling, R.M., Franklin, J., 2020. The palaeo-agulhas plain: Temporal and spatial variation in an extraordinary extinct ecosystem of the Pleistocene of the Cape floristic region. Quat. Sci. Rev. 235, 106161. https://doi.org/10.1016/J.QUASCIREV.2019.106161.
McCulloch, G., Brooks, C., Eckardt, F.D., Perkins, J.S., Atlhopheng, J.R., Meyer, T., Arntzen, J., 2010. Chapter 4 Ecology and Hydrogeology. Makgadikgadi Framework Management Plan, vol. 2. Gaborone.
Mcculloch, G.P., 2004. The Ecology of Makgadikgadi Salt Pans, Botswana and its Flamingo Populations.
McFarlane, M.J., Eckardt, F.D., 2006. Lake Deception: a new Makgadikgadi palaeolake. Botsw. Notes Rec. 38, 195–201.
McFarlane, M.J., Long, C.W., 2015. Pan floor "barchan" mounds, Ntwetwe Pan, Makgadikgadi, Botswana: their origin and palaeoclimatic implications. Quat. Int. 372, 108–119. https://doi.org/10.1016/j.quaint.2014.10.008.
McFarlane, M.J., Segadika, P., 2001. Archaeological evidence for the reassessment of the ages of the Makgadikgadi palaeolakes. Botsw. Notes Rec. 33, 83–92.
Mejdahl, V., 1979. Thermoluminescence dating: beta-dose attenuation in quartz grains. Archaeometry 21, 61–72.
Moernaut, J., Verschuren, D., Charlet, F., Kristen, I., Fagot, M., De Batist, M., 2010. The seismic-stratigraphic record of lake-level fluctuations in Lake Challa: hydrological stability and change in equatorial East Africa over the last 140 kyr. Earth Planet Sci. Lett. 290, 214–223. https://doi.org/10.1016/j.epsl.2009.12.023.
Moore, A.E., 1999. A reappraisal of epeirogenic flexure axes in southern Africa. S. Afr. J. Geol. 102, 363–376.
Moore, A.E., Cotterill, F.P.D., Eckardt, F.D., 2012. The evolution and ages of Makgadikgadi palaeo-lakes: consilient evidence from kalahari drainage evolution south-central Africa. S. Afr. J. Geol. 115, 385–413. https://doi.org/10.2113/gssajg.115.3.385.
Murray, A.S., Wintle, A.G., 2003. The single aliquot regenerative dose protocol: potential for improvements in reliability. Radiat. Meas. 37, 377–381.
Naidoo, R., Chase, M.J., Beytell, P., Du Preez, P., Landen, K., Stuart-Hill, G., Taylor, R., 2016. A newly discovered wildlife migration in Namibia and Botswana is the longest in Africa. Oryx 50, 138–146. https://doi.org/10.1017/S0030605314000222.
Papadimitrios, K.S., Bank, C.-G., Walker, S.J., Chazan, M., 2019. Palaeotopography of a Palaeolithic landscape at Bestwood 1, South Africa, from ground-penetrating radar and magnetometry. S. Afr. J. Sci. 115. https://doi.org/10.17159/sajs.2019/4793.
Pekel, J.F., Cottam, A., Gorelick, N., Belward, A.S., 2016. High-resolution mapping of global surface water and its long-term changes. Nature 540, 418–422. https://doi.org/10.1038/nature20584.
Perkins, J.S., Mcculloch, G.P., Brooks, C., Eckardt, F.D., Meyer, T., Crews, K., Bradley, J., 2010. Range Ecology, ume 2. Makgadikadi Management Plan, Gaborone.

Prescott, J.R., Hutton, J.T., 1994. Cosmic ray contributions to dose rates for luminescence and ESR dating: large depths and long-term time variations. Radiat. Meas. 23, 497–500. https://doi.org/10.1016/1350-4487(94)90086-8.
R-Development-Core-Team, 2020. A Language and Environment for Statistical Computing.
Richards, J., Burrough, S., Wiggs, G.S.F., Hills, T., Thomas, D.S.G., Moseki, L., 2021. Uneven surface moisture as a driver of dune formation on ephemeral lake beds under conditions similar to the present day: a model-based assessment from the Makgadikgadi basin, northern Botswana. Earth Surf. Process. Landforms 46, 3078–3095.
Ringrose, S., Huntsman-Mapila, P., Kampunzu, A.B., Downey, W., Coetzee, S., Vink, B., Matheson, W., Vanderpost, C., 2005. Sedimentological and geochemical evidence for palaeo-environmental change in the Makgadikgadi subbasin, in relation to the MOZ rift depression. Botswana. Palaeogeogr. Palaeoclimatol. Palaeoecol. 217 (3–4), 265–287.
Robbins, L.H., Murphy, M.L., Brook, G.A., Ivester, A.H., Campbell, A.C., Klein, R.G., Milo, R.G., Stewart, K.M., Downey, W.S., Stevens, N.J., 2000. Archaeology, palaeoenvironment, and chronology of the Tsodilo Hills white Paintings rock shelter, northwest Kalahari desert, Botswana. J. Archaeol. Sci. 27, 1085–1113.
Robbins, L.H., 1987. Stone age archaeology in the northern kalahari, Botswana: savuti and kudiakam Pan. Curr. Anthropol. 28, 567–569.
Robbins, L.H., Campbell, A.C., 1989. The depression rock shelter, Tsodilo Hills. Botsw. Notes Rec 20, 1–3.
Robbins, L.H., Campbell, A.C., Murphy, M.L., Brook, G.A., Liang, F., Skaggs, S.A., Srivastava, P., Mabuse, A.A., Badenhorst, S., 2008. Recent archaeological research at Toteng, Botswana: early domesticated livestock in the Kalahari. J. African Archaeol. 6, 131–149.
Robbins, L.H., Murphy, M.L., 1998. The early and middle stone age. In: Lane, P., Reid, A., Segobye, A. (Eds.), Ditswa Mmung: the Archaeology of Botswana. Pula Press, Gaborone, pp. 50–64.
Robbins, L.H., Murphy, M.L., Brook, G.A., Ivester, A.H., Campbell, A.C., Klein, R.G., Milo, R.G., Stewart, K.M., Downey, W.S., Stevens, N.J., 2000. Archaeology, palaeoenvironment, and chronology of the Tsodilo Hills white Paintings rock shelter, northwest Kalahari desert, Botswana. J. Archaeol. Sci. 27, 1085–1113. https://doi.org/10.1006/jasc.2000.0597.
Roberts, P., Prendergast, M.E., Janzen, A., Shipton, C., Blinkhorn, J., Zech, J., Crowther, A., Sawchuk, E.A., Stewart, M., Ndiema, E., Petraglia, M., Boivin, N., 2020. Late Pleistocene to Holocene human palaeoecology in the tropical environments of coastal eastern Africa. Palaeogeogr. Palaeoclimatol. Palaeoecol. 537, 109438. https://doi.org/10.1016/j.palaeo.2019.109438.
Russell, N.J., Armitage, S.J., 2012. A comparison of single-grain and small aliquot dating of fine sand from Cyrenaica, northern Libya. Quat. Geochronol. 10, 62–67. https://doi.org/10.1016/j.quageo.2012.03.005.
Scerri, E.M.L., Spinapolice, E.E., 2019. Lithics of the North African middle stone age: assumptions, evidence and future directions. J. Anthropol. Sci. 97, 9–43. https://doi.org/10.4436/jass.97002.
Schlebusch, C., Loog, L., Groucutt, H.S., King, T., Rutherford, A., Barbieri, C., Barbujani, G., Chikhi, L., Stringer, C., Jakobsson, M., Eriksson, A., Manica, A., Tishkoff, S.A., Scerri, E.M.L., Scally, A., Brierley, C., Thomas, M.G., 2021. Human origins in Southern African palaeo-wetlands? : strong claims from weak evidence. J. Archaeol. Sci. 130. https://doi.org/10.1016/j.jas.2021.105374.
Schmidt, M., Fuchs, M., Henderson, A.C.G., Kossler, A., Leng, M.J., Mackay, A.W., Shemang, E., Riedel, F., 2017. Paleolimnological features of a mega-lake phase in the Makgadikgadi basin (kalahari, Botswana) during marine isotope stage 5 inferred from diatoms. J. Paleolimnol. 58, 373–390. https://doi.org/10.1007/s10933-017-9984-9.
Scholz, C.A., Cohen, A.S., Johnson, T.C., King, J., Talbot, M.R., Brown, E.T., 2011. Scientific drilling in the great rift valley: the 2005 lake Malawi scientific drilling project - an overview of the past 145,000years of climate variability in southern hemisphere east Africa. Palaeogeogr. Palaeoclimatol. Palaeoecol. 303, 3–19. https://doi.org/10.1016/j.palaeo.2010.10.030.
Scholz, C, Johnson, T, Cohen, A, 2007. East African megadroughts between 135 and 75 thousand years ago and bearing on early-modern human origins. PNAS 104 (42), 16416–16421.
Schoville, B.J., Brown, K.S., Wilkins, J., 2022. A lithic provisioning model as a proxy for landscape mobility in the southern and middle kalahari. J. Archaeol. Method Theor 29, 162–187. https://doi.org/10.1007/s10816-021-09507-9.
Shaw, P.A., Stokes, S., Thomas, D.S.G., Davies, F.B.M., Holmgren, K., 1997. Palaeoecology and age of a quaternary high lake level in the Makgadikgadi basin of the middle kalahari. Botswana. S. Afr. J. Sci. 93 (6), 273–276.
Shaw, P.A., Thomas, D.S.G., 1988. Lake caprivi: a late quaternary link between the Zambezi and middle kalahari drainage systems. Zeitschrift fur Geomorphol 32, 329–337.
Shaw, P.A., Thomas, D.S.G., 1996. The quaternary palaeoenvironmental history of the kalahari, southern Africa. J. Arid Environ. 32 (1), 9–22.
Shaw, P.A., Thomas, D.S.G., Nash, D.J., 1992. Late quaternary fluvial activity in the dry valleys (mekgacha) of the middle and southern kalahari, southern Africa. J. Quat. Sci. 7, 273–281.
Singarayer, S.J., Burrough, L.S., 2015. Interhemispheric dynamics of the African rainbelt during the late Quaternary. Quaternary Science Reviews 124, 48–67.
Stager, J, Ryves, D, Chase, B, 2011. Catastrophic drought in the Afro-Asian monsoon region during Heinrich event 1. Science 331 (6022), 1299–1302. https://doi.org/10.1126/science.1198322.
Staurset, S., Coulson, S., 2014. Sub-surface movement of stone artefacts at white Paintings shelter, Tsodilo Hills, Botswana: implications for the middle stone age chronology of central southern Africa. J. Hum. Evol. 75, 153–165. https://doi.org/10.1016/j.jhevol.2014.04.006.
Staurset, S., Coulson, S.D., Mothulatshipi, S., Burrough, S.L., Nash, D.J, Thomas, D.S.G, 2022b. (under review) Post-depositional disturbance and spatial organization at exposed open-air sites: examples from the Middle Stone Age of the Makgadikgadi Basin. Quaternary Science Reviews Special Issue.
Staurset, S., Coulson, S.D., Mothulatshipi, S., Burrough, S.L., Nash, D.J, Thomas, D.S.G, 2022a. (under review) Making points: the middle stone age lithic industry of the Makgadikgadi basin, Botswana. Quaternary Science Reviews Special Issue.
Thomas, D.S.G., Burrough, S.L., Parker, A.G., 2012. Extreme events as drivers of early human behaviour in Africa? The case for variability, not catastrophic drought. J. Quat. Sci. 27, 7–12. https://doi.org/10.1002/jqs.1557.
Thomas, D.S.G., Shaw, P.A., 1992. The Zambezi River: tectonism, climatic change and drainage evolution: is there really evidence for a catastrophic flood? A discussion. Palaeogeogr. Palaeoclimatol. Palaeoecol. 91, 175–178.
Thomsen, K.J., Murray, A.S., Buylaert, J.P., Jain, M., Hansen, J.H., Aubry, T., 2016. Testing single-grain quartz OSL methods using sediment samples with independent age control from the Bordes-Fitte rockshelter (Roches d'Abilly site, Central France). Quat. Geochronol. 31, 77–96. https://doi.org/10.1016/j.quageo.2015.11.002.
Thomsen, K.J., Murray, A.S., Jain, M., Bøtter-Jensen, L., 2008. Laboratory fading rates of various luminescence signals from feldspar-rich sediment extracts. Radiat. Meas. 43, 1474–1486. https://doi.org/10.1016/j.radmeas.2008.06.002.
Vainer, Shlomy, Matmon, Ari, Hidy, Alan, J, Crouvi, Onn, De Wit, Mike, Geller, Yona, ASTER Team, 2021. Landscape responses to intraplate deformation in the Kalahari constrained by sediment provenance and chronology in the Okavango Basin. Basin Res. 33 (2), 1170–1193.
Van Waarden, C., 2010. Chapter 9 Archaeological and Other Heritage Resources. Makgadikgadi Framework Plan, ume 2. Gaborone.
Vickery, K.J., Eckardt, F.D., Bryant, R.G., 2013. A sub-basin scale dust plume source frequency inventory for southern Africa, 2005-2008. Geophys. Res. Lett. 40, 5274–5279. https://doi.org/10.1002/grl.50968.
Viehberg, F.A., Just, J., Dean, J.R., Wagner, B., Franz, S.O., Klasen, N., Kleinen, T., Ludwig, P., Asrat, A., Lamb, H.F., Leng, M.J., Rethemeyer, J., Milodowski, A.E., Claussen, M., Schäbitz, F., 2018. Environmental change during MIS4 and MIS 3 opened corridors in the Horn of Africa for Homo sapiens expansion. Quat. Sci. Rev. 202, 139–153. https://doi.org/10.1016/j.quascirev.2018.09.008.
Walker, S.J.H., Lukich, V., Chazan, M., 2014. Kathu Townlands: a high density earlier stone age locality in the interior of South Africa. PLoS One 9. https://doi.org/10.1371/journal.pone.0103436.
White, K., Eckardt, F., 2006. Geochemical mapping of carbonate sediments in the Makgadikgadi basin, Botswana using moderate resolution remote sensing data. Earth Surf. Process. Landforms 31, 665–681.
Wilkins, J., 2017. Middle Pleistocene lithic raw material foraging strategies at Kathu Pan 1, Northern Cape, South Africa. J. Archaeol. Sci. Reports 11, 169–188. https://doi.org/10.1016/j.jasrep.2016.11.002.
Wilkins, J., 2021. Homo sapiens origins and evolution in the Kalahari Basin, southern Africa. Evol. Anthropol. Issues News Rev. 30, 327–344. https://doi.org/10.1002/evan.21914.
Wurz, S., 2020. The Early Middle Stone Age in South Africa. https://doi.org/10.1093/acrefore/9780190854584.013.118.
Yellen, J.E., Brooks, A.S., 1989. The late stone age archaeology of the !kwanga and/Xai/Xai valleys. Ngamiland. Botsw. Notes Rec. 20, 5–27.